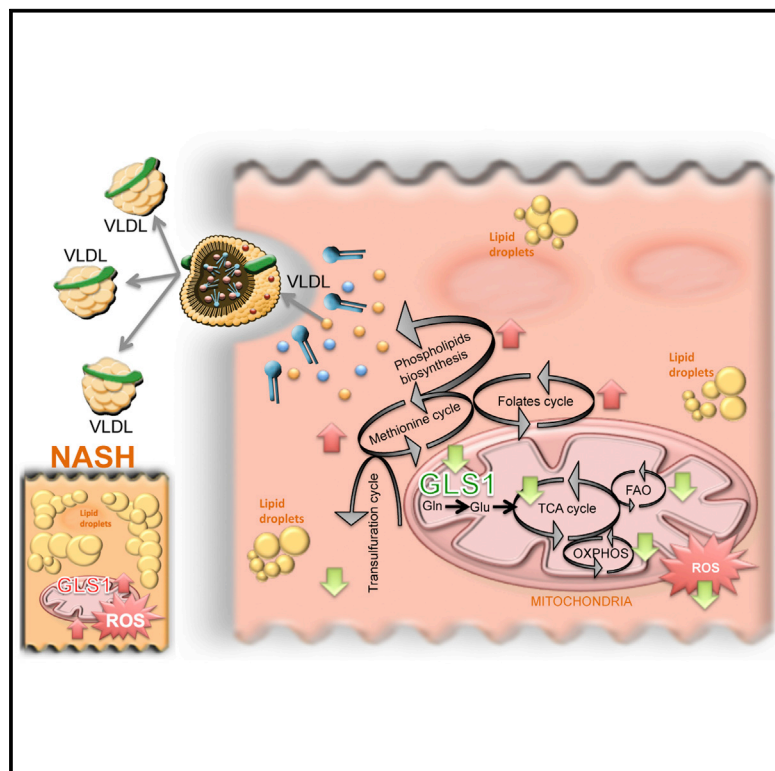# Targeting Hepatic Glutaminase 1 Ameliorates Non-alcoholic Steatohepatitis by Restoring Very-Low-Density Lipoprotein Triglyceride Assembly

Graphical Abstract

Authors

Jorge Simon, Maitane Nuñez-García, Pablo Fernández-Tussy, ..., Patricia Aspichueta, Teresa C. Delgado, María Luz Martínez-Chantar

Correspondence

tcardoso@cicbiogune.es (T.C.D.), mlmartinez@cicbiogune.es (M.L.M.-C.)

In Brief

Simon et al. show that the glutaminase GLS1 isoform is augmented in both NASH clinical biopsies and pre-clinical mouse models. GLS1 silencing significantly reduced steatosis and oxidative stress through complex metabolic reprogramming, involving increased VLDL export, indicating that GLS1 may be a valuable therapeutic target for the treatment of NASH.

Highlights

- The high activity glutaminase isoform, GLS1, is augmented in NASH

- GLS1 inhibition reduces steatosis in NASH by increasing VLDL export

- GLS1 inhibition diminishes oxidative stress in pre-clinical models of NASH

- GLS1 targeting may be a valuable therapeutic approach in NASH

CellPress

Targeting Hepatic Glutaminase 1 Ameliorates Non-alcoholic Steatohepatitis by Restoring Very-Low-Density Lipoprotein Triglyceride Assembly

Jorge Simon,[1] Maitane Nuñez-García,[2] Pablo Fernández-Tussy,[1] Lucía Barbier-Torres,[1] David Fernández-Ramos,[1]
Beatriz Gómez-Santos,[2] Xabier Buqué,[2,3] Fernando Lopitz-Otsoa,[1] Naroa Goikoetxea-Usandizaga,[1]
Marina Serrano-Macia,[1] Rubén Rodriguez-Agudo,[1] Maider Bizkarguenaga,[1] Imanol Zubiete-Franco,[1]
Virginia Gutiérrez-de Juan,[1] Diana Cabrera,[4] Cristina Alonso,[5] Paula Iruzubieta,[6,7]

(Author list continued on next page)

[1]Liver Disease Laboratory, Liver Metabolism Laboratory, Center for Cooperative Research in Biosciences (CIC bioGUNE), Basque Research and Technology Alliance (BRTA), Centro de Investigación Biomédica en Red de Enfermedades Hepáticas y Digestivas (CIBERehd), 48160 Derio, Bizkaia, Spain
[2]Department of Physiology, Faculty of Medicine and Nursing, University of the Basque Country (UPV/EHU), 48940 Leioa, Bizkaia, Spain
[3]Biocruces Health Research Institute, 48903 Barakaldo, Bizkaia, Spain
[4]Metabolomics Platform, Center for Cooperative Research in Biosciences (CIC bioGUNE), Basque Research and Technology Alliance (BRTA), Centro de Investigación Biomédica en Red de Enfermedades Hepáticas y Digestivas (CIBERehd), 48160 Derio, Bizkaia, Spain
[5]Owl Metabolomics, 48610 Derio, Bizkaia, Spain
[6]Gastroenterology and Hepatology Department, Marqués de Valdecilla University Hospital, 39008 Santander, Spain
[7]Clinical and Traslational Digestive Research Group, Instituto de Investigación Sanitaria Valdecilla (IDIVAL), 39011 Santander, Spain
[8]Unit for the Clinical Management of Digestive Diseases, Hospital Universitario Virgen del Rocío, CIBERehd, University of Seville, 41013 Seville, Spain
[9]Department of Physiology, Center for Research in Molecular Medicine and Chronic Diseases (CIMUS), University of Santiago de Compostela-Instituto de Investigación Sanitaria, CIBER Fisiopatología de la Obesidad y Nutrición (CIBERobn), Galician Agency of Innovation (GAIN), Xunta de Galicia, 15782 Santiago de Compostela, Spain

(Affiliations continued on next page)

SUMMARY

Non-alcoholic steatohepatitis (NASH) is characterized by the accumulation of hepatic fat in an inflammatory/fibrotic background. Herein, we show that the hepatic high-activity glutaminase 1 isoform (GLS1) is overexpressed in NASH. Importantly, GLS1 inhibition reduces lipid content in choline and/or methionine deprivation-induced steatotic mouse primary hepatocytes, in human hepatocyte cell lines, and in NASH mouse livers. We suggest that under these circumstances, defective glutamine fueling of anaplerotic mitochondrial metabolism and concomitant reduction of oxidative stress promotes a reprogramming of serine metabolism, wherein serine is shifted from the generation of the antioxidant glutathione and channeled to provide one-carbon units to regenerate the methionine cycle. The restored methionine cycle can induce phosphatidylcholine synthesis from the phosphatidylethanolamine N-methyltransferase-mediated and CDP-choline pathways as well as by base-exchange reactions between phospholipids, thereby restoring hepatic phosphatidylcholine content and very-low-density lipoprotein export. Overall, we provide evidence that hepatic GLS1 targeting is a valuable therapeutic approach in NASH.

INTRODUCTION

Non-alcoholic fatty liver disease (NAFLD) is a global health problem with an estimated worldwide prevalence of 30%–40% of the adult population (Younossi et al., 2016). It includes a group of conditions characterized by the accumulation of fat in the liver

Context and Significance

Non-alcoholic steatohepatitis (NASH) is a global health problem and risk factor for cirrhosis, liver cancer, and cardiovascular diseases. Currently, regardless of huge investments made by researchers and pharmaceutical industry, there are still no approved therapies for the treatment of NASH. Herein, investigators of CIC bioGUNE in Spain and colleagues have studied the role of the amino acid glutamine and its catabolism in NASH. They show that a liver enzyme involved in glutamine metabolism, glutaminase 1, is elevated in hepatic biopsies of NASH patients and in mouse models of the disease. Therapeutically, they reveal that GLS1 inhibition in pre-clinical models reduces liver steatosis and oxidative stress without side effects. Overall, GLS1 targeting could be a valuable therapeutic approach for the clinical management of NASH.

Manuel Romero-Gomez,[8] Sebastiaan van Liempd,[4] Azucena Castro,[5] Ruben Nogueiras,[9] Marta Varela-Rey,[1]
Juan Manuel Falcón-Pérez,[4,10] Erica Villa,[11] Javier Crespo,[6,7] Shelly C. Lu,[12] Jose M. Mato,[1] Patricia Aspichueta,[2,3]
Teresa C. Delgado,[1,*] and María Luz Martínez-Chantar[1,13,*]

[10]Ikerbasque, Basque Foundation for Science, 48013 Bilbao, Bizkaia, Spain
[11]Department of Gastroenterology, Azienda Ospedaliero-Universitaria & University of Modena and Reggio Emilia, 41121 Modena, Italy
[12]Division of Digestive and Liver Diseases, Department of Medicine, Cedars-Sinai Medical Center, Los Angeles, CA 90048, United States
[13]Lead Contact
*Correspondence: tcardoso@cicbiogune.es (T.C.D.), mlmartinez@cicbiogune.es (M.L.M.-C.)

resulting from a metabolic reprogramming, which can include (1) increased fatty acid uptake; (2) reduced mitochondrial fatty acid beta-oxidation (FAO), the catabolic process by which fatty acids are metabolized; (3) increased de novo lipogenesis synthesis of fatty acids; (4) and/or disruptions in the very-low-density lipoprotein (VLDL) assembly and secretion, particles that account for the hepatic triglycerides, cholesterol, and apolipoproteins exported from the liver to peripheral tissues. Patients with simple steatosis, a condition usually considered rather benign on the NAFLD spectrum, have excellent prognosis from a liver standpoint. On the other hand, non-alcoholic steatohepatitis (NASH), a more aggressive form that is characterized by necroinflammation and fibrosis localized on the most harmful part of the spectrum of NAFLD progression, is an important risk factor for cirrhosis and liver cancer (Ascha et al., 2010), one of the deadliest and fastest-increasing types of cancer, as well as for cardiovascular diseases, which are major causes of global mortality (Söderberg et al., 2010). Pharmacological approaches targeting NASH should ideally block progression and reverse liver injury. However, in spite of the huge investment by the pharmacological industry over the last years, there are still no approved therapies targeting NASH (Cassidy and Syed, 2016). Weight loss and exercise are the only effective therapeutic approaches, but compliance remains a problem.

Dysfunctional VLDL synthesis and secretion is a hallmark of NASH (Fujita et al., 2009). Hepatic VLDL assembly and secretion is a complex process involving apoliprotein B (ApoB), microsomal triglyceride transfer protein (MTP), and lipid mobilizing and synthesizing proteins, particularly phospholipids (Eisenberg and Olivecrona, 1979). Indeed, rare ApoB and MTP mutations are associated with progressive liver disease (Cefalù et al., 2013; Di Filippo et al., 2014). Likewise, feeding rodents a diet deficient in choline, a substrate of the synthesis of the main phospholipid forming the VLDL particle membranes, phosphatidylcholine (Ptd-Cho), results in the accumulation of fat in the liver (Caballero et al., 2010). Exclusively in the liver, Ptd-Cho can be additionally synthesized from the methylation of phosphatidylethanolamine (Ptd-Et), a reaction catalyzed by the enzyme phosphatidylethanolamine N-methyltransferase (PEMT) that uses S-adenosylmethionine (SAMe), an intermediate of the methionine cycle, as the methyl donor (Noga et al., 2002). On this basis, $Pemt^{-/-}$ mice present disrupted VLDL triglyceride export and are more prone to develop liver steatosis (Zhao et al., 2009). Likewise, both mice deficent for methionine adenosyltransferase 1a ($Mat1a^{-/-}$) and mice maintained on a methionine-deficient diet have chronically low levels of SAMe and spontaneously develop NASH as a consequence of an impaired PEMT pathway and hepatic VLDL assembly (Caballero et al., 2010; Cano et al., 2011; Chen et al., 2010; Mato et al., 2013). This is relevant to human NAFLD, as about 50% of NAFLD patients present a serum metabolic signature associated with $Mat1a^{-/-}$ mice (Alonso et al., 2017), indicating that impaired VLDL assembly may be present in a subtype of NAFLD patients.

The nutritional model of feeding a diet deficient in both methionine and choline (MCD) is characterized by macrovesicular steatosis, hepatocellular death, inflammation, oxidative stress, and fibrosis. Even though there are discrepancies between this model and human NASH, with weight loss, the lack of peripheral insulin resistance, and hypoglycemia being the most confounding factors, this model is often used in NASH research, as short-term dietary interventions are associated with NASH. Using this animal model, Li and colleagues have found significant changes in the serum levels of glutamine (Li et al., 2011). L-glutamine is the most abundant free amino acid in the human body, and some reports have highlighted the beneficial protective effects of oral glutamine supplementation on the development of NASH (Sellmann et al., 2015). In the liver, glutaminase (EC 3.5.1.2) is the main regulator enzyme of glutamine metabolism and catalyzes the first step of glutamine catabolism through the conversion of glutamine to glutamate and ammonia. There are two different phosphate-activated glutaminase isoforms, GLS2 and GLS1. The GLS2 gene, located on chromosome 12, encodes two splice variants with a low activity and allosteric regulation, liver-type glutaminase (LGA, short transcript isoform), and glutaminase B (GAB, long transcript isoform), which are highly expressed in normal adult liver (Matés et al., 2013). Likewise, the GLS1 gene, located in chromosome 2, encodes two splice variants with a high activity and low Km, kidney-type glutaminase (KGA, long transcript isoform) and the glutaminase C (GAC, short transcript isoform), which is mainly expressed in the kidney under healthy conditions. Notably, a metabolic switch from the GLS2 to GLS1 isoform occurs in cirrhosis and liver cancer (Yu et al., 2015; Yuneva et al., 2012). More recently, Du and colleagues have shown that GLS1 is induced in fibrotic livers, and inhibition of glutaminase blocked the activation of hepatic stellate cells (HSCs), the major hepatic cell type involved in fibrosis, halting fibrosis progression (Du et al., 2018). In a similar way, the scavenging of the toxic side product of glutaminase, ammonia, has been shown to be important for preventing fibrosis progression (Canbay and Sowa, 2019; De Chiara et al., 2019). In spite of this, the relevance of the expression of GLS1 isoform in NAFLD is poorly understood. A previous study has shown that treatment of hepatoma cells with phenylbutyrate, a glutamine scavenger, reduced the palmitate-mediated induction of triglycerides levels by decreasing endoplasmic reticulum (ER) stress (Rahman et al., 2009). In agreement with this, the hepatic metabolism of the amino acid glutamine has been previously

implicated in the regulation of cellular redox balance in the pathophysiology of numerous diseases as glutamine can be used as an anaplerotic substrate to support mitochondrial metabolism (Alberghina and Gaglio, 2014; Faubert et al., 2014). Here, we show that GLS1 is overexpressed in NASH, both in the clinical setting and in pre-clinical mouse models, and, more importantly, we show that specific GLS1 inhibition accounts for reduced liver steatosis and oxidative stress. Under conditions of methionine and choline deprivation, usually characterized by impaired VLDL export, GLS1 inhibition lowered oxidative stress and restored Ptd-Chol synthesis and VLDL triglyceride export, thereby reducing liver steatosis. Overall, hepatic GLS1 targeting is suggested as a valuable therapeutic approach in NASH.

RESULTS

Glutaminase 1 (GLS1) Is Overexpressed in Clinical Non-alcoholic Steatohepatitis

High-throughput metabolomics is a widely used method to investigate metabolic phenotypes in specific conditions. Here, we screened serum levels of glutamine and the glutaminase reaction product, glutamate, in a large cohort of patients (Barr et al., 2012). Whereas there are no significant differences in serum glutamine levels between controls (n = 90) and NASH patients (n = 131), serum glutamate levels are significantly increased in NASH patients (Figure 1A), suggesting that glutamine catabolism may be aberrant in NASH. Glutaminase is the main regulator enzyme of hepatic glutamine catabolism, catalyzing the conversion of glutamine to glutamate and ammonia (the latter is excreted by the urea cycle). Whereas GLS2 is the major isoform expressed in the healthy liver, a switch from GLS2 to GLS1 occurs in liver fibrosis (Du et al., 2018), cirrhosis, and liver cancer (Yu et al., 2015; Yuneva et al., 2012). Herein, a group of patients diagnosed with NASH, characterized in Table S1, show increased hepatic GLS1 levels relative to healthy controls. Likewise, in another cohort of patients with NASH, mRNA levels of GLS1 were shown to be increased relative to healthy controls. Under these conditions, the isoform 2 of glutaminase, GLS2, usually distributed around the hepatic periportal compartment in healthy people, is decreased in the livers of NASH patients. In addition, glutamine synthetase, usually expressed in the perivenous hepatocytes of healthy livers, catalyzing the synthesis of glutamine from glutamate and elimination of residual ammonia that escapes from detoxification in the periportal hepatocytes, is induced (Figures 1B and 1C).

Overall, we provide evidence that hepatic GLS1 expression is increased in NASH patients.

Glutaminase 1 (GLS1) Is Overexpressed in Mouse Models of Non-alcoholic Steatohepatitis

Taking into consideration the relevance of GLS1 expression in clinical NASH, we have evaluated GLS1 expression in an in vivo pre-clinical mouse model of NASH, the mice fed a choline and methionine deficient diet. Even though this model presents some constraints, it is one of the most often used models in NASH research. Herein, the choline-deficient and 0.1% methionine diet (0.1% MCDD) was used, as one of the limitations of a methionine and choline-deficient diet is the rapid weight loss.

Adding 0.1% methionine prevents this (Iruarrizaga-Lejarreta et al., 2017). Animals fed a 0.1% MCDD rapidly accumulate hepatic fat in the form of macrovesicular steatosis and progress to inflammation and fibrosis, hallmarks of NASH, after 2, 4, and 6 weeks of the diet, respectively (Figure S1A). To confirm that fibrosis is not significant at 4 weeks of 0.1% MCDD, we have measured gene expression of fibrotic markers, such as Acta2 (actin alpha 2) and Timp1 (tissue inhibitor of metalloproteinases-1), that were not significantly altered after 4 weeks of 0.1% MCDD (data not shown). Moreover, earlier evidence has highlighted that GLS1 expression is increased with advanced tumor grade and therefore dedifferentiation (Li et al., 2018). Herein, animals fed a 0.1% MCDD over the course of four weeks do not present alterations in dedifferentiation parameters such as albumin, alpha-fetoprotein, and the transcription factor hepatocyte nuclear factor 4 (HNF4), at least as assessed by mRNA levels (Figure S1B).

Importantly, animals maintained on a 0.1% MCDD show a time-dependent increase in GLS1 expression, both at the protein and the mRNA level (Figures 2A–2C). Furthermore, staining of consecutive slides from liver biopsy of an animal fed a 0.1% MCDD for 4 weeks shows that GLS1 staining does not overlap with F4/80 staining (a marker of KC) and fibrosis areas (Sirius red staining). On the other hand, after 6 weeks of 0.1% MCDD, liver biopsies show co-staining of GLS1 and Sirius red staining (Figure 2D). In agreement, after four weeks of 0.1% MCDD, the accumulation of GLS1 is mainly localized in hepatocytes, as shown by double immunofluorescence, where GLS1 co-localizes with Albumin, a hepatocyte marker, and not with αSMA, an HSC marker (Figure 2E). As a positive control of GLS1 staining, we show co-localization of GLS1 and albumin in mouse liver tumors (Figures S2A and S2B). On the other hand, the expression of the GLS2 isoform of glutaminase, usually distributed around the periportal regions, is reduced in steatotic livers (Figures 2A–2C and S2C). Likewise, in a NASH model of 8-month-old Mat1a⁻/⁻ mice (Alonso et al., 2017; Cano et al., 2011), GLS1 liver expression is induced together with glutamine synthetase, whereas GLS2 is reduced (Figure S2D).

In addition, we have evaluated the expression of glutamine metabolism key regulators in a mouse model of mice fed a choline-deficient, high-fat diet (CD-HFD). Previous reports have shown that this mouse model develops NASH in a similar pattern to that observed in humans, showing hepatic ballooning and fibrosis, with concomitant obesity as well as dyslipidemia and insulin resistance (Wolf et al., 2014). After six weeks of CD-HFD, we observed increased body weight in these animals relative to the standard chow (SC) diet-fed age-matched rodents (Figure S3A). Hepatic triglycerides are increased, and hepatic inflammation is significant, although serum transaminases and triglycerides are not significantly altered (Figures S3B–S3G). Finally, after six-weeks of CD-HFD, hepatic fibrosis is not significant (Figure S3B). Similar to what occurs in the 0.1% MCDD-fed rodents, CD-HFD-fed animals present decreased VLDL triglyceride export (Figure S3H). Importantly, GLS1 levels are induced after as little as three weeks of CD-HFD (Figures S3I and S3J).

Overall, we provide evidence that hepatic GLS1 expression is increased in mouse models of NASH.
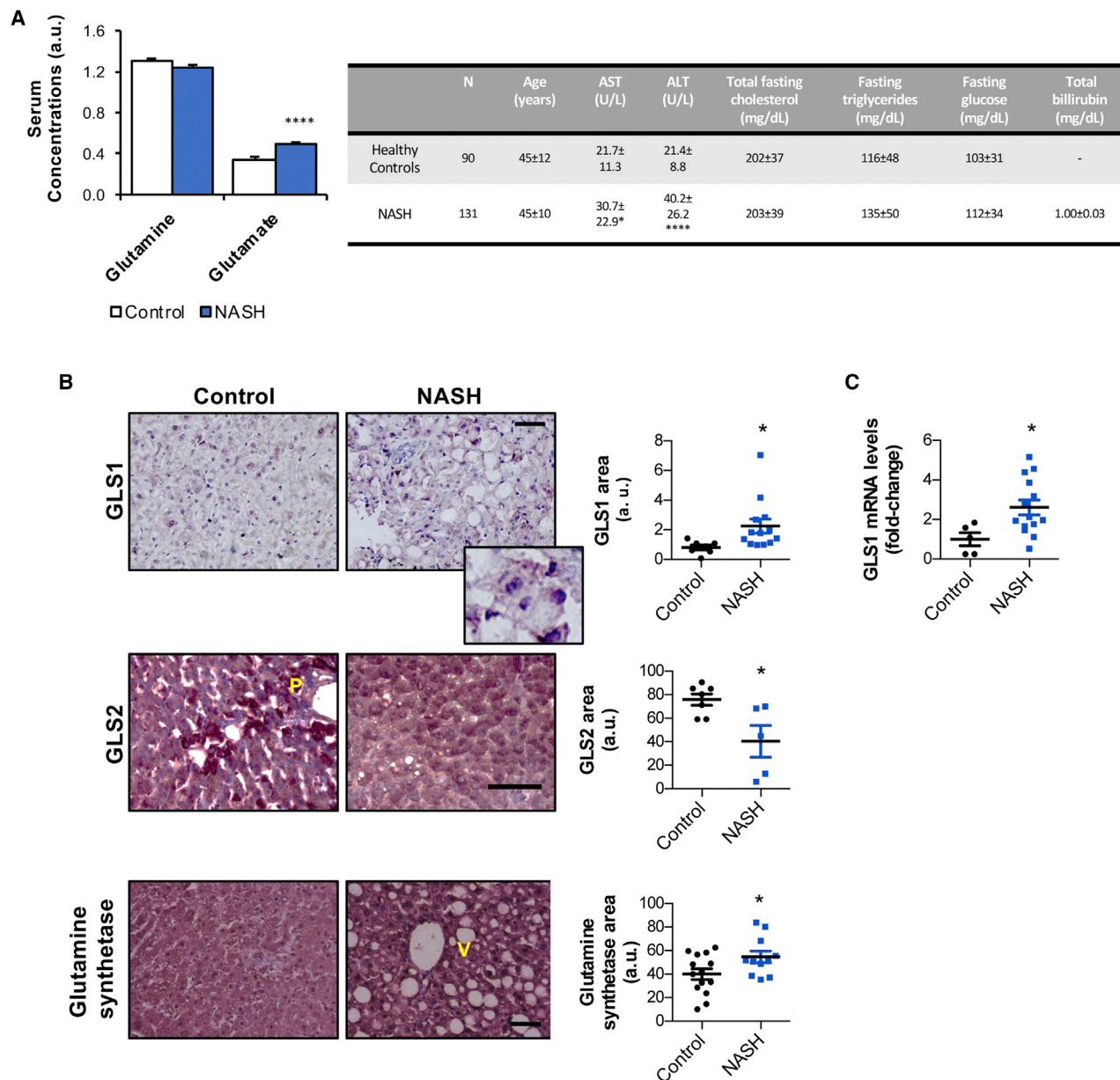
Figure 1. Glutaminase 1 (GLS1) Is Overexpressed in Clinical Non-alcoholic Steatohepatitis

(A) Serum levels of glutamine and the product of glutamine catabolism, glutamate, in a large cohort of patients diagnosed with NASH (n = 131) relative to a control group of healthy subjects (n = 90). A table showing the main serum biochemical parameters relative to these patients is shown.

(B) Liver immunohistochemical staining and respective quantification for the isoform 1 of glutaminase (GLS1), and inset zoom, the isoform 2 of glutaminase (GLS2) and glutamine synthetase in another cohort of NASH patients (n = 13) versus a control group of healthy subjects (n = 13). Scale bar corresponds to 100 μm. V, venous region; P, portal region.

(C) mRNA levels of *GLS1* in a cohort of NASH patients (n = 16) against a control group of age- and body-weight matched healthy controls (n = 5). Data are shown as average ± SEM, and Student's t test was used to compare groups. *p < 0.05 and ****p < 0.0001 against the control group are shown (see also Table S1).

Targeting Glutaminase 1 (GLS1) *In Vitro* Resolves Hepatocyte Lipid Accumulation

Based on recent reports suggesting the important role of GLS1 in HSC during fibrosis progression (Du et al., 2018), particularly in animals treated with carbon tetrachloride (CCl₄), we aimed at identifying the main hepatic cells where GLS1 expression is induced in mouse models of NASH as a result of choline and methionine deprivation. Thus, after 4 weeks of 0.1% MCDD, a

time point where inflammation is present and fibrosis is not significant (Figure S1A), we perfused mouse livers to isolate hepatocytes as well as liver stroma cells, namely HSC and the liver-resident macrophages, the Kupffer cells (KCs). We compared the expression of GLS1 in the different hepatic populations of 0.1% MCDD-fed rodents relative to animals fed an SC diet. We found that mRNA levels of *Gls1* are significantly increased in isolated hepatocytes from animals maintained on a 0.1%

A 0.1% MCDD

B 0.1% MCDD

C

D

E
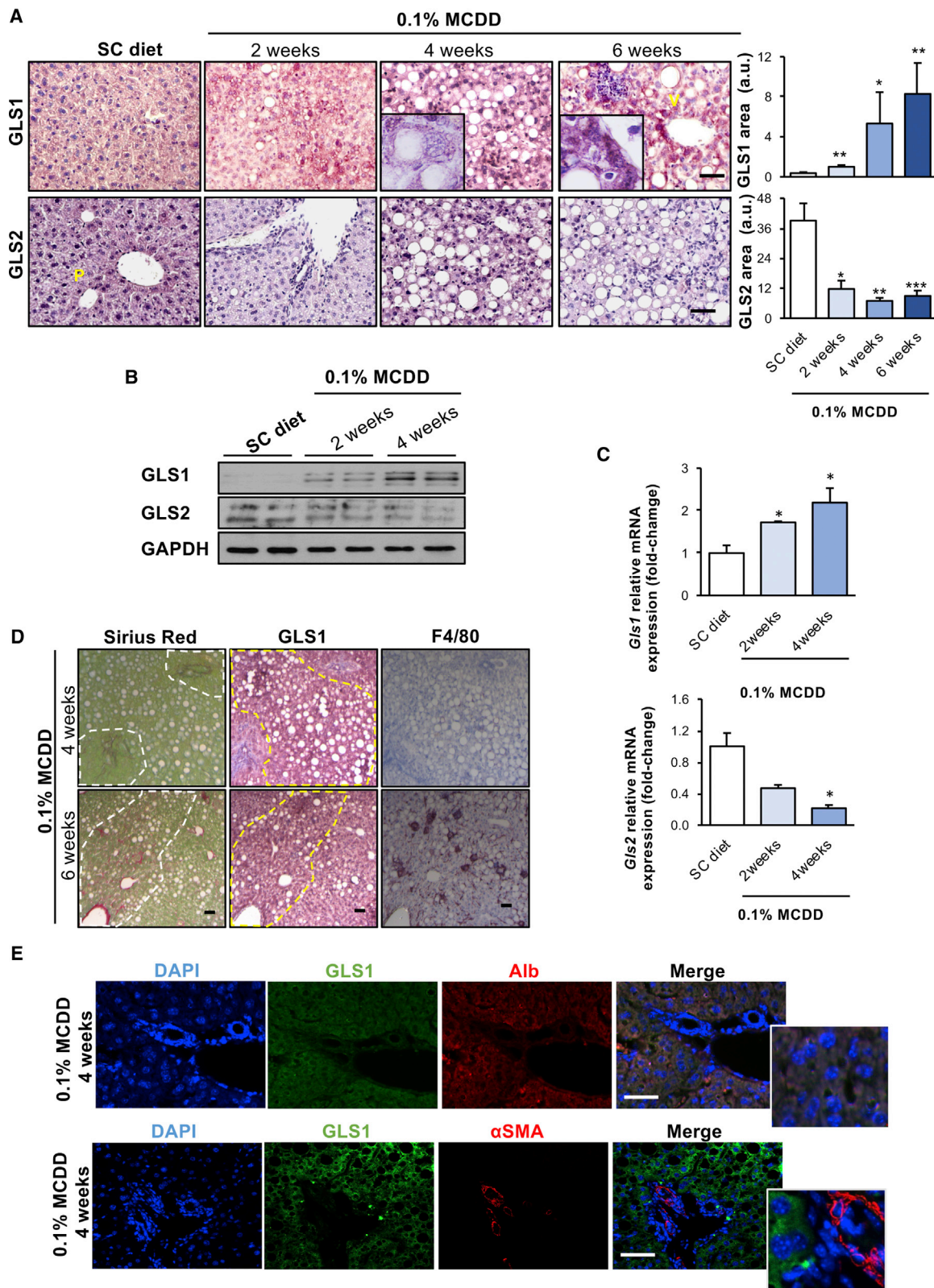
(legend on next page)

MCDD relative to the controls, whereas no changes were observed in either HSC or KC (Figure S4A). Likewise, in cultured primary mouse HSC, which undergo activation *in vitro*, *Gls1* mRNA levels are increased after 7 days of culture, corresponding to an increase in the activation of HSC (Zubiete-Franco et al., 2017). On the other hand, *Gls1* mRNA levels are not significantly induced in cell cultures of primary mouse KC after stimulation with lipopolysaccharide (LPS) (Figures S4B and S4C). Overall, these results show that glutamine catabolism in the hepatocyte is relevant in our mouse model of NASH, although the relevance of other hepatic cell types for the net induction of GLS1 levels in the livers must be taken into consideration in NASH models presenting a higher degree of fibrosis.

In order to further assess the relevance of the high-activity glutaminase GLS1 isoform expression in the hepatocytes during NASH, primary mouse hepatocytes were isolated. Primary cultures of hepatocytes represent substantial limitations that include dedifferentiation. As expected, and in agreement with previous evidence (Li et al., 2018), GLS1 is gradually increased during culture (Figure S4D). Isolated mouse hepatocytes were maintained on a methionine- and choline-deficient (MCD) medium that has been previously shown to induce steatosis and injury in the hepatocyte cell line AML-12 (Sahai et al., 2006) as well as in primary mouse hepatocytes (Iruarrizaga-Lejarreta et al., 2017). Under conditions of MCD treatment, GLS1 was inhibited *in vitro* by using either molecular approaches (siRNA) or the small pharmacological inhibitor BPTES (Bis-2-(5-phenylacetamido-1,3,4-thiadiazol-2-yl)ethyl sulfide). BPTES is an allosteric, time-dependent, and specific inhibitor of GLS1 that exhibits unique binding at the oligomerization interface of the glutaminase tetramer (DeLaBarre et al., 2011; Thangavelu et al., 2012; Thomas et al., 2013). *Gls1* silencing in primary hepatocytes cultured for 48 h in MCD media reduced the accumulation of triglycerides (Figures 3A–3C and S5A). Likewise, the pharmacological inhibition of GLS1 by using BPTES, as detected by the decreased cellular glutamate/glutamine ratio, significantly reduced the accumulation of triglycerides (Figures S5B–S5D). Under these conditions, cell viability, as assessed by caspase activity, was not significantly altered after *Gls1* silencing or pharmacological inhibition by using BPTES (Figure S5E). In addition, *GLS1* silencing in a human hepatocyte cell line, the THLE-2 cells, also reduces lipid accumulation after MCD treatment (Figure S5F), whereas in isolated mouse hepatocytes incubated in the presence of oleic acid, a cell model where hepatocytes accumulate lipids due to increase uptake and also inhibition of VLDL export (Nossen et al., 1986), both GLS1 silencing and pharma-cological inhibition using BPTES also reduce hepatocytes lipid content (Figure S5G).

Finally, when we silenced *Gls1* in mouse hepatocytes treated with MCD media, dedifferentiation parameters, such as albumin, alpha-fetoprotein, and HNF4, were unaltered at the mRNA level. (Figure S5H).

Taken together, GLS1 silencing ameliorates steatosis in isolated hepatocytes.

Targeting Glutaminase 1 (GLS1) *In Vivo* Resolves Non-alcoholic Steatohepatitis

Taking into consideration that GLS1 is increased in NASH, the potential therapeutic role of silencing *Gls1 in vivo* was assessed. Thus, we have evaluated the effects of *Gls1* silencing in mice fed a 0.1% MCDD. Depriving mice of methionine and choline for four weeks caused an increase in hepatic content of fatty acids, cholesteryl esters, diglycerides, and triglycerides. As expected, the concentration of serum triglycerides and cholesterol was reduced, attributable to a phosphatidylcholine-related defect in hepatic VLDL secretion, as previously described (Rizki et al., 2006; Table S2). Liver histology confirmed marked lipid accumulation after four weeks of 0.1% MCDD (Figure 3D). In addition, four weeks of 0.1% MCDD lowered blood glucose (Table S2).

Hepatic *Gls1* was silenced in 0.1% MCDD-fed rodents by using twice-a-week tail vein injections of Invivofectamine conjugated to either *Gls1*-specific or Control siRNA, from weeks 2 to 4 of 0.1% MCDD. As a result of *Gls1* silencing, GLS1 hepatic levels are reduced and GLS2 expression is increased, whereas glutamine synthetase expression is not significantly altered at the protein level (Figures 3D, S6A, and S6B). Of relevance, the levels of hepatic ammonia, a secondary product of the glutaminase reaction, are not significantly altered after *Gls1* silencing (Table S2). Under these circumstances, reduced glutaminase activity was confirmed by measuring the incorporation of ^{13}C labeling from glutamine into glutamate, confirming that glutaminase activity is, on one hand, induced in the diet, and on the other, there is a tendency for decreased glutaminase activity after *Gls1* silencing *in vivo* (Figure S6C). Importantly, GLS1-specific silencing *in vivo*, both at the protein and the mRNA level, significantly reduced liver steatosis, measured as Sudan red staining and by biochemical assay (Figure 3D; Table S2). Furthermore, *Gls1* silencing *in vivo* in 0.1% MCDD-fed rodents significantly increased hepatic phospholipid content while decreasing cholesteryl esters and restoring serum triglyceride levels (Table S2).

Finally, in animals fed a CD-HFD for 6 weeks, we have silenced GLS1 by using twice-a-week tail vein injections of

Figure 2. Glutaminase 1 (GLS1) Is Overexpressed in a Mouse Model of Non-alcoholic Steatohepatitis of Choline-Deficient and 0.1% Methionine-Diet (0.1% MCDD)-Fed Rodents

(A) Hepatic glutaminase 1 (GLS1), with higher magnification zoom shown in inset, and glutaminase 2 (GLS2) immunostaining and respective quantifications. Scale bar corresponds to 100 μm. V, venous region; P, portal region.

(B) Hepatic GLS1 and GLS2 protein levels by western blot analysis. Glyceraldehyde-3-phosphate (GAPDH) was used as a loading control.

(C) Hepatic *Gls1* and *Gls2* mRNA levels in mice fed a choline-deficient and 0.1% methionine diet (0.1% MCDD) against a standard chow diet (SC diet) during 2, 4, and 6 weeks. Data are shown as average ± SEM, and Student's t test was used to compare groups. *p < 0.05, **p < 0.01, and ***p < 0.001 are shown versus age- and gender-matched animals maintained on SC diet.

(D) Representative consecutive slides staining for GLS1, F4/80 and Sirius red staining in liver biopsies of animals maintained for 4 or 6 weeks on 0.1% MCDD (fibrosis areas highlighted with white dashed line and GLS1 with yellow dashed line).

(E) Immunofluorescence double co-staining for GLS1 and albumin, a marker of hepatocytes, and alpha smooth muscle actin (αSMA), a marker of hepatic stellate cells (HSCs), in 0.1% MCDD-fed mice for 4 weeks (see also Figures S1–S4).
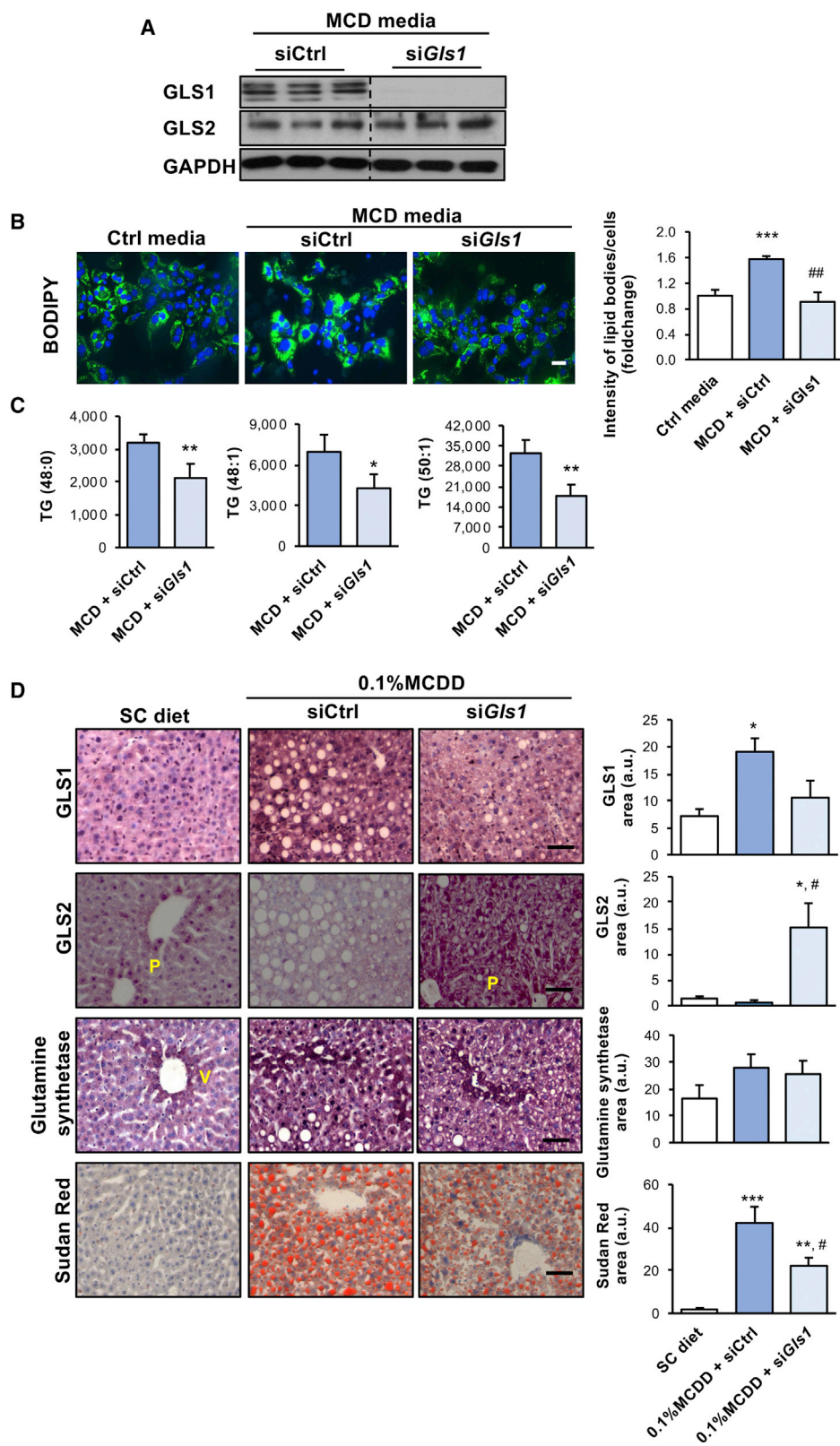
(legend on next page)

Invivofectamine conjugated to either *Gls1*-specific or control siRNA from weeks 3 to 6 of CD-HFD (Figures S6D and S6E). In these animals, *Gls1* silencing was able to significantly reduce hepatic steatosis (Figures S6F and S6G) without changes to body weight and food intake (data not shown).

In summary, GLS1 inhibition ameliorates liver steatosis in preclinical mouse models of NASH.

Targeting Glutaminase 1 (GLS1) *In Vitro* and *In Vivo* Restores Very-Low-Density Lipoprotein (VLDL) Export after Methionine and Choline Deprivation

As mentioned before, phospholipids are required for correct VLDL assembly, and therefore, methionine and choline deprivation results in impaired VLDL export. Taking that into account, the impact of *Gls1* silencing in Ptd-Chol synthesis and VLDL export was evaluated both *in vitro* and *in vivo*. First, hepatocytes grown for 48 h in complete and MCD media under conditions of *Gls1* or control silencing were incubated with (U-^{13}C)glucose for 1 h. Using mass spectrometry, we have measured the incorporation of the glucose tracer in intracellular Ptd-Chol species. Under conditions of choline and methionine deprivation, there is a tendency for reduced incorporation of carbon tracers in Ptd-Chol, reflecting impaired Ptd-Chol synthesis from glucose. On the other hand, *Gls1* silencing under conditions of methionine and choline deprivation promoted the synthesis of some Ptd-Chol species (Figure S7A). Moreover, we treated isolated mouse hepatocytes with lomitapide, described previously to inhibit MTP and shown to hinder VLDL export (Sirtori et al., 2014). As expected, treatment with lomitapide caused the accumulation of cell lipids to a similar extent in cells treated with complete and methionine- and choline-deficient media. Interestingly, under these conditions, *Gls1* silencing does not prevent cell lipid accumulation after lomitapide treatment, suggesting that *Gls1* silencing-induced lipid lowering may somehow be related to VLDL export (Figure 4A).

In addition, hepatic phospholipid content was determined in mice maintained on a diet deprived of methionine and choline and after control or *Gls1* silencing. We observed that as a result of *in vivo Gls1* silencing in 0.1% MCDD-fed rodents, hepatic Ptd-Cho and phosphatidylserine (Ptd-Ser) levels are augmented, whereas Ptd-Et levels remain unaltered (Figure 4B). Thus, we decided to evaluate the composition of the secreted VLDL particles in mice fed a 0.1% MCDD and where we have silenced *Gls1*. For this, circulating VLDL catabolism was inhibited through the administration of poloxamer 407, a non-

ionic detergent described to inhibit lipoprotein lipase (LPL) (Millar et al., 2005), an enzyme mostly abundant in tissues involved in fatty acid metabolism, such as muscle and adipose tissue (Karpe et al., 1998). When we silence *Gls1 in vivo* in mice fed a 0.1% MCDD, the lipid content of the secreted VLDL particles was significantly enriched in lipids, such as triglycerides, phospholipids, and cholesterol derivatives (Figure 4C). In spite of this, the number of VLDL particles, determined by the VLDL secretion rate and the molecules of apoB secreted, was not altered (Figures S7B and S7C). Likewise, in mice fed a CD-HFD for six weeks, *Gls1* silencing results in a tendency for increased VLDL triglyceride content in VLDL isolated from vena cava serum after 2 h of fasting (Figure S7D).

Overall, we provide evidence that *Gls1* silencing ameliorates liver steatosis by targeting VLDL assembly through mechanisms that have not been previously explored.

Targeting Glutaminase 1 (GLS1) *In Vitro* and *In Vivo* Reduces Oxidative Stress

Oxidative stress plays a crucial role in the pathogenesis and progression of NASH. In agreement, we have observed that harvesting the primary mouse hepatocytes with media deprived of methionine and choline increases both total and mitochondrial reactive oxygen species (ROS) levels (Figure 5A). Reduced glutathione (GSH) is considered to be one of the most important ROS scavengers. Importantly, the ratio between GSH and oxidized glutathione (GSSG) may be used as a marker of oxidative stress. Thus, four weeks of 0.1% MCDD is associated with augmented GSSG/GSH ratio and increased incorporation of labeled glutamine into GSH, highlighting that GSH synthesis is increased under these conditions and reverted under *Gls1* silencing conditions (Figure 5B). GSSG/GSH is also reduced under GLS1 silencing conditions in mice fed a CD-HFD (Figure 5C). Likewise, the total levels of malondialdehyde (MDA), a marker of lipid peroxidation, were induced (Figure 5D). Noteworthy, *Gls1* silencing significantly reduces oxidative stress in primary hepatocytes and in the *in vivo* NASH models (Figures 5A–5D).

Numerous causes of oxidative stress have been associated with NASH. Impaired tricarboxylic acid (TCA) cycle, FAO, and oxidative phosphorylation (OXPHOS) originate ROS (Rosca et al., 2012; van de Wier et al., 2013). Here, we have measured hepatic TCA cycle activity, evaluated as the incorporation of U-^{13}C-glutamine into 1-^{13}C-citrate; hepatic FAO, measured using radioactive incorporation of labeled palmitate into CO_2 and

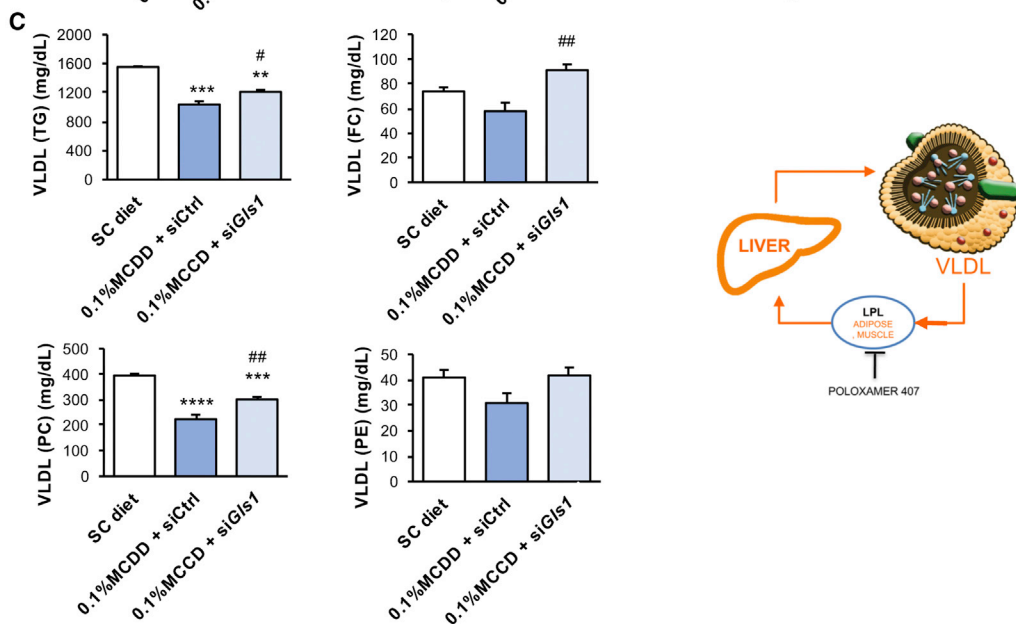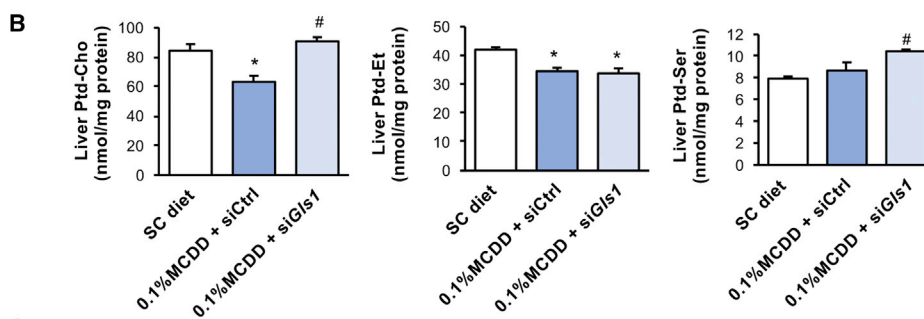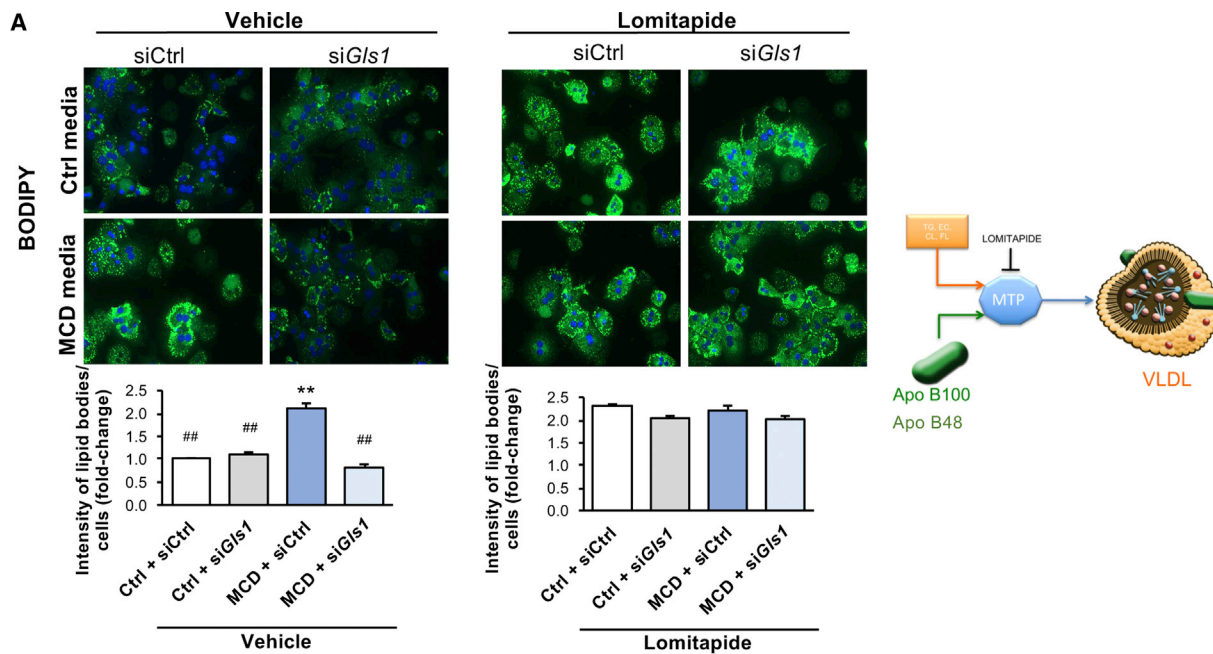**Figure 3. Targeting Glutaminase 1 (GLS1) *In Vitro* and *In Vivo* Resolves the Accumulation of Hepatic Triglycerides and Non-alcoholic Steatohepatitis**

(A) Western blot analysis of total protein levels of glutaminase 1 (GLS1) and glutaminase 2 (GLS2). Glyceraldehyde-3-phosphate dehydrogenase (GAPDH) was used as a loading control.

(B) Representative BODIPY staining micrographs and respective quantification. Scale bar corresponds to 100 μm.

(C) Mass spectrometry analysis of different triglyceride (TG) isoforms in mouse isolated hepatocytes treated for 48 h with methionine- and choline-deficient media (MCD) after treatment with siRNA against *Gls1* (si*Gls1*) or unrelated control (siCtrl). At least triplicates were used for each experimental condition. Data are shown as average ± SEM, and Student's t test was used to compare between the groups. *p < 0.05 and ***p < 0.001 versus MCD + siCtrl and ##p < 0.01 versus mcd + siCtrl are shown.

(D) GLS1, GLS2, and glutamine synthetase levels quantified by immunohistochemistry and representative micrographs of Sudan Red staining and respective quantification in animals maintained on a choline-deficient and 0.1% methionine diet (0.1% MCDD). From weeks 2 to 4 of diet, two different experimental groups were treated either with siCtrl or si*Gls1*. Scale bar corresponds to 100 μm. At least n = 5 were used for each experimental group. Data are shown as average ± SEM, and one-way ANOVA followed by Bonferroni post-test were used to compare between multiple groups. *p < 0.05, **p < 0.01, and ***p < 0.001 versus SC diet and #p < 0.05 versus 0.1% MCDD + siCtrl are shown (see also Figures S4–S6 and Table S2).

A

Vehicle

siCtrl | siGls1

Lomitapide

siCtrl | siGls1

BODIPY

Ctrl media

MCD media

Intensity of lipid bodies/cells (fold-change)

Vehicle

Intensity of lipid bodies/cells (fold-change)

Lomitapide

LOMITAPIDE

MTP

Apo B100
Apo B48

VLDL

B

Liver Ptd-Cho (nmol/mg protein)

SC diet | 0.1%MCDD + siCtrl | 0.1%MCDD + siGls1

Liver Ptd-Et (nmol/mg protein)

SC diet | 0.1%MCDD + siCtrl | 0.1%MCDD + siGls1

Liver Ptd-Ser (nmol/mg protein)

SC diet | 0.1%MCDD + siCtrl | 0.1%MCDD + siGls1

C

VLDL (TG) (mg/dL)

SC diet | 0.1%MCDD + siCtrl | 0.1%MCCD + siGls1

VLDL (FC) (mg/dL)

SC diet | 0.1%MCDD + siCtrl | 0.1%MCCD + siGls1

VLDL (PC) (mg/dL)

SC diet | 0.1%MCDD + siCtrl | 0.1%MCCD + siGls1

VLDL (PE) (mg/dL)

SC diet | 0.1%MCDD + siCtrl | 0.1%MCCD + siGls1

LIVER

VLDL

LPL
ADIPOSE, MUSCLE

POLOXAMER 407

(legend on next page)

into incompletely oxidized acid-soluble metabolites (ASM); as well as mitochondrial oxidative phosphorylation (OXPHOS), as measured by oxygen consumption rate (OCR) using a Seahorse analyzer. All the analyzed parameters were significantly higher after four weeks of 0.1% MCDD, and, importantly, *Gls1* silencing during 0.1% MCDD restored TCA, β-oxidation, and OXPHOS pathway fluxes to control diet levels in association with reduced oxidative stress (Figures 5E–5G).

In summary, targeting hepatic GLS1 *in vitro* and *in vivo* reduces ROS levels by reducing oxidative metabolism.

Glutaminase 1 (GLS1)-Mediated Reduction of Oxidative Stress Is Associated with Restored Hepatic Phospholipid Content

Choline is essential for the *de novo* synthesis of Ptd-Chol, the major phospholipid component of plasma lipoproteins, via the cytidine-diphosphate pathway (CDP). Decreased hepatic Ptd-Chol reduces the levels of circulating VLDL (Cole et al., 2012). In the liver, Ptd-Cho can be additionally synthesized from the methylation of Ptd-Et, a reaction catalyzed by the enzyme PEMT and using SAMe, an intermediate of the methionine cycle, as a methyl donor (Noga et al., 2002). The other intermediate of the methionine cycle, homocysteine, at the crossroads of the metabolic pathways, is either degraded via the transsulfuration pathway to cysteine and then GSH or is remethylated back to methionine. Indeed, depletion of SAMe and increased GSH synthesis are early events in the MCD model of NASH (Caballero et al., 2010) (Table S3; Figure 5B).

In one carbon metabolism, a carbon unit from serine or glycine is transferred to tetrahydrofolate (THF) to form methylene-THF (MTHF). MTHF either can be used for the synthesis of purines or reduced to methyl-THF, which can be used to methylate homocysteine to methionine. Likewise, serine, which has previously been shown to be able to transfer one-carbon units to recycle homocysteine to methionine in tumor cells (Maddocks et al., 2016), can be used in combination with homocysteine to synthesize GSH or can be metabolized to Ptd-Ser by Ptd-ser synthase II (PTDSS2) (Kuge and Nishijima, 1997; Kuge et al., 1997). In mammals, Ptd-Ser can be further metabolized to Ptd-Et and later converted to Ptd-Chol by PEMT activity. Then, Ptd-Cho can undergo a base-exchange process with Ptd-Ser, releasing choline through the exchange with serine. Thus, even under conditions of choline deprivation, newly formed choline can be metabolized to Ptd-Cho through the CDP-choline pathway (Maldonado et al., 2014).

We have previously shown that *Gls1* silencing on 0.1% MCDD-fed mice reduced oxidative stress and decreased GSH synthesis (Figure 5B). In agreement, the expression of the genes involved in the transsulfuration pathway are reduced after *Gls1* silencing, whereas expression of enzymes involved in the folate and methionine cycles is augmented (Figure 6A). Likewise, the mRNA levels of the genes involved in the CDP-choline and CDP-ethanolamine pathways and the enzymes catalyzing the base-exchange among the different phospholipids are induced after *Gls1* silencing (Figure 6B). Although *Pemt* mRNA expression is not upregulated after *Gls1* silencing, the increase in the Ptd-Cho/Ptd-Et ratio observed (1.4 ± 0.3 in 0.1% MCDD + si*Gls1* versus 1.0 ± 0.25 in 0.1% MCDD + siCtrl, $p < 0.01$) can be indicative of increased PEMT activity that relies on the transfer of methylation units.

These results indicate that GLS1-mediated reduction of oxidative stress is associated with restored hepatic phospholipid content.
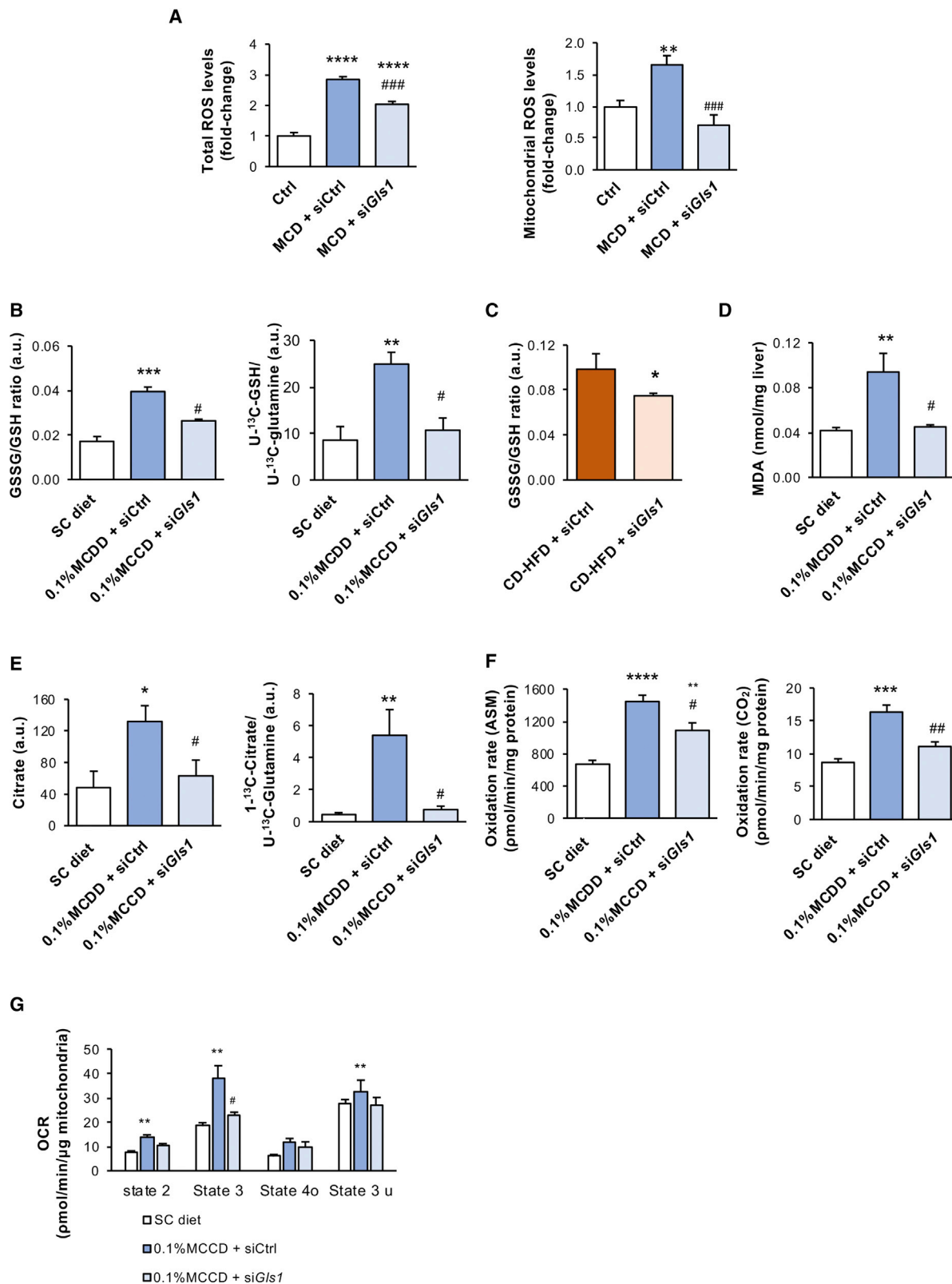
DISCUSSION

Therapeutic solutions to address the major health problem of NASH are a hot topic. Recent reports have highlighted the importance of glutamine catabolism in liver disease, namely in fibrosis, cirrhosis, and HCC (Du et al., 2018; Yu et al., 2015; Yuneva et al., 2012). In the liver, glutaminase is the main regulator of glutamine catabolism, catalyzing the conversion of glutamine to glutamate and ammonia. In recent years, a metabolic switch from the low-activity GLS2 isoform to the high-activity GLS1 isoform was observed in end stages of chronic liver disease (Du et al., 2018; Yu et al., 2015; Yuneva et al., 2012). Herein, we have shown higher hepatic expression of GLS1 in NASH patients. Moreover, we have shown that during NASH progression, the upregulation of GLS1 occurs at the mRNA level. Previously, other studies have shown that there are many factors related to the induction of GLS1 during cancer progression: (1) c-Myc (Gao et al., 2009), (2) K-Ras mutations (Brunelli et al., 2014), (3) the splicing factor *SLU7* (Elizalde et al., 2014), (4) elevated mitochondrial phosphorous levels under hypoxic conditions commonly found in the tumor microenvironment (Cassago et al., 2012), and (5) oncogenic diffuse β cell lymphoma protein in an NF-κB (nuclear factor kappa-light-chain-enhancer of activated B cells)-dependent manner (Wang et al., 2010). Related to this, further studies are necessary to better understand the mechanism underlying GLS1 upregulation in NASH.

Figure 4. Targeting Glutaminase 1 (GLS1) *In Vitro* and *In Vivo* Restores Very-Low-Density Lipoprotein (VLDL) Triglyceride Export after Choline and Methionine Deprivation

(A) Representative BODIPY staining micrographs and respective quantification in mouse isolated hepatocytes treated with control media (Ctrl) or methionine- and choline-deficient media (MCD) for 24 h after overnight treatment with siRNA against *Gls1* (si*Gls1*) or unrelated control (siCtrl). In some experimental conditions, lomitapide was added at 600 nM for 24 h. Scale bar corresponds to 100 μm. At least triplicates were used for each experimental condition. Data are shown as average ± SEM, and one-way ANOVA followed by Bonferroni post-test was used to compare between groups. **$p < 0.01$ versus Ctrl + siCtrl and ##$p < 0.01$ versus MCD + siCtrl are shown.

(B and C) Liver phosphatidylcholine (Ptd-Cho), phosphatidylethanolamine (Ptd-Et), and phosphatidylserine (Ptd-Ser) hepatic levels (B) and (C) serum very-low-density lipoprotein (VLDL) phospholipids and lipid content (TG, triglycerides, FC, free cholesterol, PC, phosphatidylcholine, PE, phosphatidylethanolamine) in mice fed either a standard chow (SC) diet or a diet deficient in choline with 0.1% methionine (0.1% MCDD) for four weeks. From weeks two to four of diet, two different experimental groups were treated either with siCtrl or si*Gls1*. Animals were administered poloxamer 407 (P407) and serum VLDL isolated and analyzed at 6 h after P407 administration. At least n = 5 were used for each experimental group. Data are shown as average ± SEM, and one-way ANOVA followed by Bonferroni post-test were used to compare between multiple groups. **$p < 0.01$, ***$p < 0.001$, and ****$p < 0.0001$ versus SC diet, and #$p < 0.05$ and ##$p < 0.01$ versus 0.1% MCDD + siCtrl are shown (see also Figure S7).

Figure 5. Targeting Glutaminase 1 (GLS1) *In Vitro* and *In Vivo* Reduces Oxidative Stress

(A) Total and mitochondrial reactive oxygen species (ROS) levels in mouse isolated hepatocytes treated with control media (Ctrl) or methionine and choline deficient media (MCD) for 48 h after overnight treatment with siRNA against *Gls1* (si*Gls1*) or unrelated control (siCtrl). At least triplicates were used for each

(legend continued on next page)

Dysfunctional VLDL synthesis and secretion is a hallmark of NASH (Fujita et al., 2009). Methionine and choline are fundamental amino acids for the synthesis of Ptd-Col, an essential phospholipid for VLDL assembly and therefore hepatic triglyceride export. On this basis, mice fed a methionine- and/or choline-deficient diet present impaired VLDL export. Despite the limitations of the mouse models of methionine and choline deprivation regarding human NASH, the most obvious of which is a lack of weight gain, the methionine- and choline-deficient nutritional model is one of the most used mouse models of NASH. Importantly, in the nutritional mouse models of 0.1% MCDD- and CD-HFD, we have observed increased hepatic GLS1 expression. Likewise, we have shown that in 8-month-old Mat1a$^{-/-}$ mice, known to have impaired VLDL export (Cano et al., 2011), GLS1 hepatic expression is induced. Even though GLS1 has recently been shown to play an important role in fueling HSC glutaminolysis and proliferation during hepatic fibrosis (Du et al., 2018), here, we have focused on the earlier stages of NASH. Thus, in animals fed a 0.1% MCDD for 4 weeks, characterized by hepatic steatosis and inflammation, we have shown that GLS1 expression is specifically induced in hepatocytes and not in stromal cells.

GLS1 expression has been previously shown to be increased with advancing tumor grade and therefore dedifferentiation (Li et al., 2018). Herein, the augmented GLS1 expression in mouse hepatocytes from a NASH background even though is not associated with changes of dedifferentiation markers, such as HNF4α, at the mRNA levels, we cannot preclude that the regulation of this transcription factor is occurring at the protein level, as it is known that post-transcriptional mechanisms play important roles in the regulation of factors such as HNF4α during hepatocyte differentiation/de-differentiation. Indeed, previous evidence from our group have shown that HNF4α was decreased in HCC derived from NASH and also in NASH patients (Frades et al., 2015). Thus, we could hypothesize that GLS1 is selectively upregulated in de-differentiated sub-populations of hepatocytes during NASH and could potentially drive HCC derived from NASH.

Taking into consideration the relevance of GLS1 during NASH pathogenesis, we have evaluated the therapeutic potential of GLS1 inhibition both in cell and in pre-clinical mouse models of NASH. First, we have observed that GLS1 inhibition effectively reduced the accumulation of fat in mouse hepatocytes, in human hepatocyte cell line, and mouse livers under methionine and/or choline deprivation. Under these circumstances, decreased steatosis was associated with augmented hepatic Ptd-Chol content that partly normalized VLDL assembly, increasing triglyceride and cholesterol export from the liver. It must be mentioned that although secreted VLDL particles are lipid enriched, serum levels of triglycerides and cholesterol after GLS1-inhibition in 0.1% MCDD-fed mice are not higher than values from healthy age- and gender-matched control mice, suggesting that serum hypertriglyceridemia and hypercholesterolemia and associated atherosclerotic complications are not a potential concern when using GLS1-targeted therapies during NASH management. As a result of GLS1 inhibition in 0.1% MCDD-fed rodents, GLS2 levels around the portal region are increased. GLS2 has been recently shown to be an essential enzyme for glucagon-induced flux from glutamine to glucose in primary hepatocytes, and Gls2$^{-/-}$ mice show reduced blood glucose levels after overnight fasting (Miller et al., 2018). These data are in agreement with our findings in which 0.1% MCDD-fed rodents, with augmented GLS1 expression and lowering of GLS2 hepatic levels, have lower blood glucose. Lower blood glucose under these conditions can also be associated with the decreased hepatic glucose production caused by glycogen depletion, as previously reported (Leclercq et al., 2007). However, this raises concerns regarding the possible adverse effects of GLS1 inhibition and concomitant GLS2 increase in promoting hyperglycemia. In spite of this, in our mouse model of 0.1% MCDD, Gls1 silencing is not associated with fasting hyperglycemia. Finally, as glutaminase accounts for the formation of glutamate and ammonia from glutamine, interventions targeting glutamine catabolism may potentially disturb ammonia homeostasis, a highly toxic by-product of this reaction that is excreted through the urea cycle. Neither four weeks of 0.1% MCDD nor Gls1 silencing under these conditions is associated with accumulation of hepatic ammonia, in agreement with previous evidence (Gutiérrez-de-Juan et al., 2017). Based on our evidence, we can speculate that as glutamine synthetase is not significantly altered in our NASH mouse model, perhaps at this time point of disease progression, the urea cycle enzymes are not decreased as occurs at later steps of the disease (De Chiara et al., 2018) and can therefore detoxify ammonia preventing its toxic accumulation.
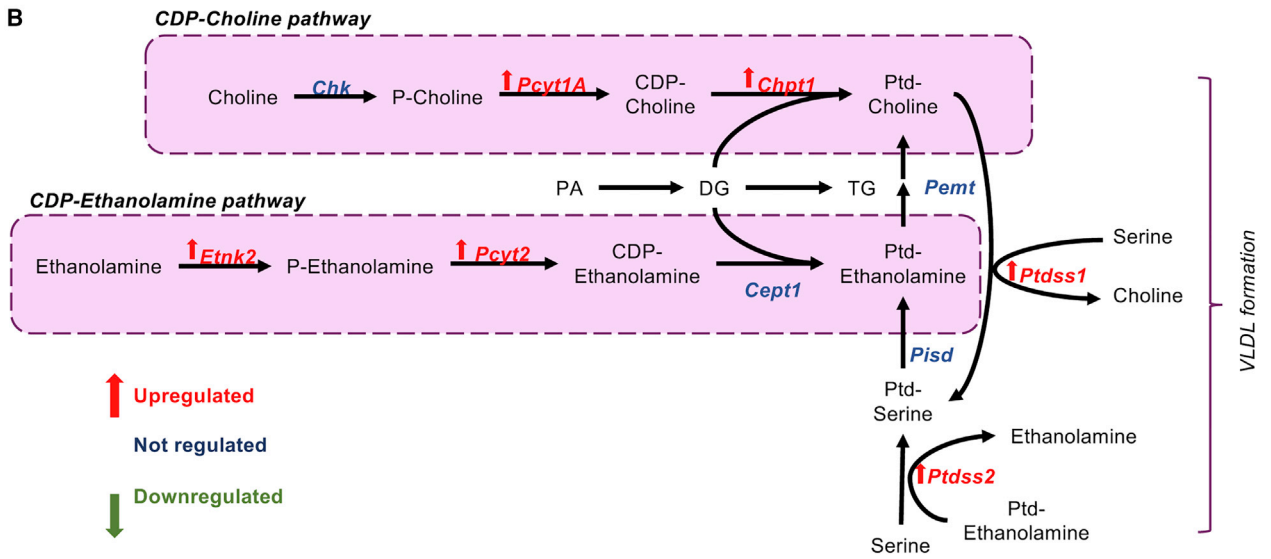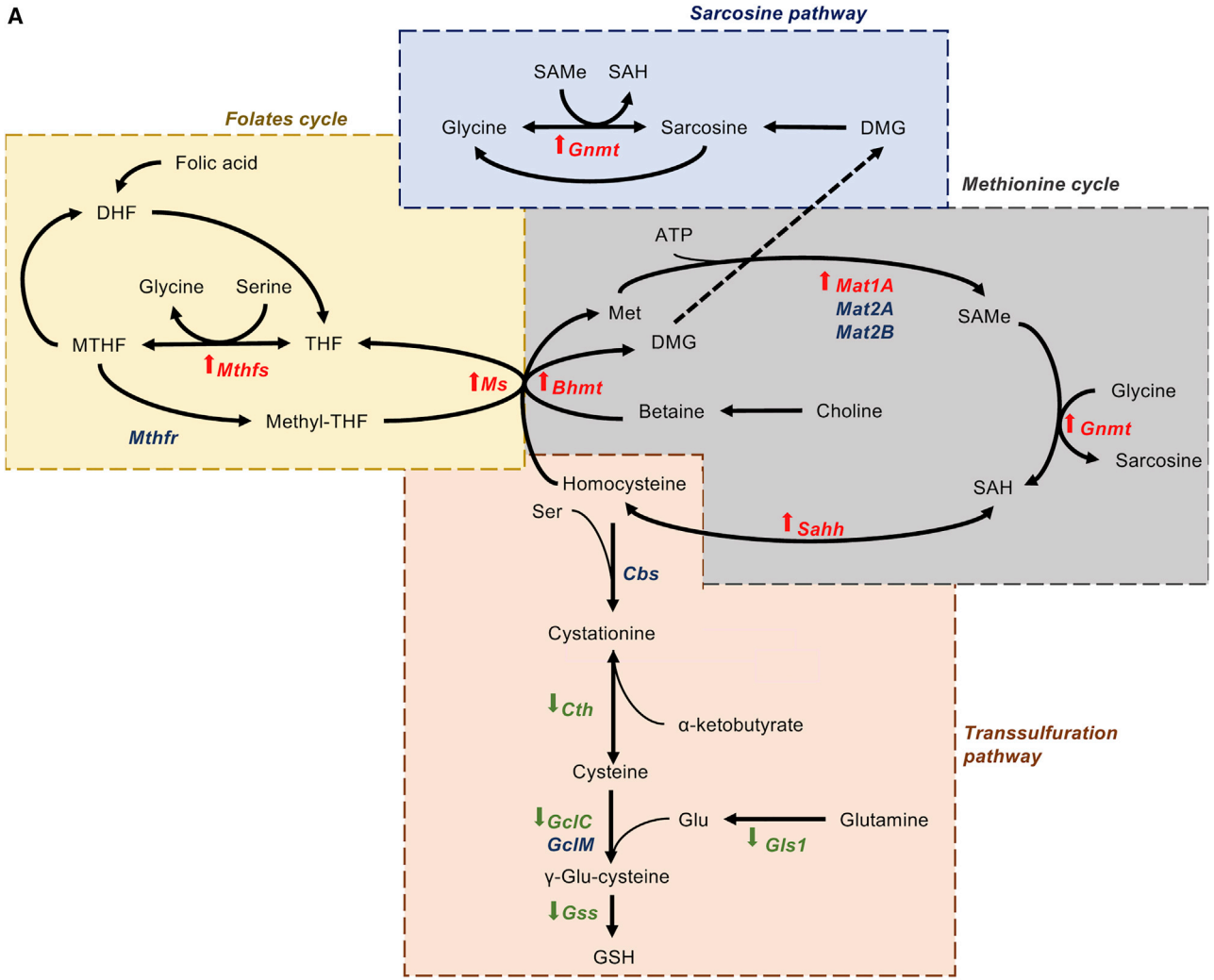
Besides disruptions of VLDL assembly and export, methionine and/or choline deprivation in rodents also blunts hepatic lipogenesis and hypermetabolism characterized by enhanced FAO

experimental condition. Data are shown as average ± SEM, and one-way ANOVA followed by Bonferroni post-test were used to compare between multiple groups. **p < 0.01 and ****p < 0.0001 versus Ctrl media as well as ###p < 0.001 versus MCD media + siCtrl are shown.
(B) Oxidized glutathione (GSSG) and reduced glutathione (GSH) ratio and incorporation of ^{13}C carbons from U-^{13}C(glutamine) carbons into 5-^{13}C(GSH) in mice fed either a standard chow diet (SC) or a diet deficient in choline with 0.1% methionine (0.1% MCDD) for four weeks. From weeks two to four of diet, two different experimental groups were treated either with siCtrl or siGls1. At least n = 5 were used for each experimental group. Data are shown as average ± SEM, and one-way ANOVA followed by Bonferroni post-test were used to compare between multiple groups. **p < 0.01 and ***p < 0.001 versus SC diet, and #p < 0.05 versus 0.1% MCDD + siCtrl are shown.
(C) Oxidized and reduced glutathione ratio (GSSG/GSH) in animals maintained on a choline-deficient and high-fat diet (CD-HFD) for 6 weeks. From week 3 to 6 of diet, two different experimental groups were treated either with siCtrl or siGls1 (CD-HFD + siCtrl or CD-HFD + siGls1). At least n = 5 were used for each experimental group. Data are shown as average ± SEM, and Student's t test was used to compare between groups. *p < 0.05 versus CD-HFD + siCtrl is shown.
(D–G) Malondialdehyde (MDA) levels as a measurement of lipid peroxidation (D); citrate and incorporation of U-^{13}C(glutamine) carbons on 1-^{13}C(citrate) levels (E); Fatty acid oxidation (FAO) rate quantified from the incorporation of ^{14}C-palmitate into CO_2 and in acid-soluble metabolites (ASM)(F); and mitochondrial oxygen consumption rate (OCR) in different states of the respiration (state 2, state 3, state 4o, state 3u) in mice fed either a standard chow diet (SC) or a diet deficient in choline with 0.1% methionine (0.1% MCDD) for four weeks. From weeks two to four of diet, two different experimental groups were treated either with siCtrl or siGls1. At least n = 5 were used for each experimental group. Data are shown as average ± SEM, and one-way ANOVA followed by Bonferroni post-test were used to compare between multiple groups. *p < 0.05, **p < 0.01, ***p < 0.001, and ****p < 0.0001 versus SC diet and #p < 0.05 and ##p < 0.01 versus 0.1% MCDD + siCtrl are shown (see also Figure S3).

A

Sarcosine pathway

SAMe → SAH

Glycine ⇄ Sarcosine ← DMG

↑ *Gnmt*

Folates cycle

Folic acid

DHF

Glycine Serine

MTHF ⇄ THF

↑ *Mthfs*

Methyl-THF

Mthfr

↑ *Ms* ↑ *Bhmt*

Methionine cycle

ATP

Met DMG ↑ *Mat1A* *Mat2A* *Mat2B* SAMe

Betaine ← Choline

Glycine

↑ *Gnmt*

Sarcosine

SAH

↑ *Sahh*

Homocysteine

Ser

Cbs

Cystationine

↓ *Cth* α-ketobutyrate

Cysteine

↓ *GclC* *GclM* Glu ← Glutamine

↓ *Gls1*

γ-Glu-cysteine

↓ *Gss*

GSH

Transsulfuration pathway

B

CDP-Choline pathway

Choline → *Chk* → P-Choline → ↑ *Pcyt1A* → CDP-Choline → ↑ *Chpt1* → Ptd-Choline

PA → DG → TG *Pemt*

CDP-Ethanolamine pathway

Ethanolamine → ↑ *Etnk2* → P-Ethanolamine → ↑ *Pcyt2* → CDP-Ethanolamine → *Cept1* → Ptd-Ethanolamine

↑ *Ptdss1* Serine / Choline

Pisd

Ptd-Serine

↑ *Ptdss2* Ethanolamine / Ptd-Ethanolamine

Serine

VLDL formation

↑ Upregulated

Not regulated

↓ Downregulated

(legend on next page)

(Rizki et al., 2006). Under these conditions, augmented FAO increases the TCA cycle anaplerotic capacity, which accounts for the replenishment of the mitochondrial carbon pool. Under these circumstances, the excessive glutamine catabolism mediated by GLS1 accounts for increased levels of glutamate, which can be further deaminated to α-ketoglutarate in order to sustain augmented TCA cycle anaplerosis. Hepatic anaplerotic pathways are energetically backed by elevated oxidative metabolism in the liver through OXPHOS, as previously observed in mice fed a choline- and methionine-deficient diet (Romestaing et al., 2008). Altogether, rises in TCA cycle anaplerosis, FAO, and OXPHOS contribute to oxidative stress during NASH (Satapati et al., 2015). These results agree with earlier clinical data showing elevated FAO (Iozzo et al., 2010) as well as in vivo splanchnic oxygen consumption and mitochondrial respiration (Felig et al., 1974; Koliaki et al., 2015) and TCA cycle activity (Hyötyläinen et al., 2016; Sunny et al., 2011) in NAFLD. Finally, Dasarathy and colleagues have shown that NASH subjects present a higher rate of synthesis of cystathionine, a precursor of GSH, from serine (Dasarathy et al., 2009). These results are in agreement with our data showing that hepatic GSH synthesis is increased after four weeks of 0.1% MCDD. Serine is a metabolite that lies at the crossroads between the synthesis of phospholipids and total GSH synthesis. In the liver, serine can be metabolized to Ptd-Ser and further metabolized to Ptd-Et and then methylated to Ptd-Chol by PEMT. Moreover, serine has been shown to be able to transfer one-carbon units to recycle homocysteine to methionine to support the methionine cycle (Maddocks et al., 2016). The methionine cycle, which is impaired after a choline- and/or methionine-deficient diet and in a subtype of NASH patients (Alonso et al., 2017), plays an important role in the biosynthesis of hepatic phospholipids by providing methyl groups for the reaction catalyzed by PEMT.

Herein, *Gls1* silencing in 0.1% MCDD-fed rodents is associated with decreased TCA cycle activity, through the reduction of the replenishment of carbon units necessary for sustaining anaplerosis. Reduced TCA cycle and associated diminishment of NADH and FADH$_2$ fueling of OXPHOS further reduce oxidative stress after GLS1 inhibition. Likewise, decreased oxidative stress is observed after *Gls1* silencing in the CD-HFD rodents. Under these circumstances, reduced oxidative stress alleviates serine usage for GSH synthesis; instead, serine is recruited to fuel the folate and methionine cycle and synthetize phospholipids via PEMT. Increased Ptd-Chol is able to induce the assembly of lipid-enriched VLDL particles and, in this way, diminish the accumulation of triglycerides and cholesterol in the liver. Finally, a decreased triglyceride content is followed by a reduction in FAO, associated with diminished TCA cycle and OXPHOS and further promoting an improvement in NASH (Figure 7).

Earlier therapeutic approaches targeting glutamine metabolism in cancer focused on scavenging glutamine usage, as for example using phenylbutyrate. Also, L-ornithine phenylacetate (OP) has been applied to the treatment of hyperammonemia and hepatic encephalopathy. The combination of L-ornithine (amino acid) with phenylacetate, reduces toxic levels of ammonia by (1) L-ornithine acting as a substrate for glutamine synthesis from ammonia in skeletal muscle and (2) phenylacetate excreting the ornithine-related glutamine as phenylacetyl-glutamine in the kidneys (Jalan et al., 2007). Currently, most therapeutic approaches regulating glutamine metabolism focus on the initial stage of glutaminolysis by inhibiting GLS1. GLS1 inhibitors, such as UPGL00004 (Huang et al., 2018), 968 (Yuan et al., 2016), BPTES (Sappington et al., 2016), CB-839 or Telaglenastat (Calithera) (Gross et al., 2014), a family of thiourea derivatives (THDP17) (Díaz -Herrero et al., 2014), ebselen (Thomas et al., 2013) and 6-diazo-5-oxo-L-norleucine (Rahman et al., 1985), effectively inhibit GLS1 by different mechanism and reduce tumor growth in vitro and in vivo. Whereas BPTES's poor aqueous solubility and unfavorable pharmacokinetic profile have hampered its clinical development (Shukla et al., 2012), BPTES-loaded polyethylenoglycol nanoparticles, a nanoencapsulation allowing the safe administration of this drug, are currently being tested in pre-clinical mouse models (Elgogary et al., 2016). Also, Telaglenastat, an orally bioavailable inhibitor, is in phase one clinical trials for the therapy in some types of cancer. In spite of this, the potential side effects of strategies impacting whole-body glutamine metabolism must be seriously considered, and interventions targeting hepatic GLS1 inhibition are preferable for NASH management.

In summary, given the paramount importance of glutamine metabolism through GLS1 in the redox control and related liver fat build-up in NASH shown here together with its role in the regulation of fibrosis progression, as previously described (Du et al., 2018), interfering with its function might represent a general mechanism for metabolic reprogramming under pathophysiological conditions and an attractive strategy for the treatment of NASH.

Limitations of Study

The primary mouse hepatocyte model used in this study shows limitations associated with the dedifferentiation of these cells

---

Figure 6. GLS1-Mediated Reduction of Oxidative Stress Is Associated with Increased Phospholipid Synthesis and the Activation of Folate and Methionine Cycles

(A) Differential expression of mRNA levels from genes significantly different involved either in glutathione (GSH) synthesis through the transsulfuration pathway, and the folates and methionine cycles in mice on a 0.1% MCDD and with *Gls1* silencing (si*Gls1*) versus control silencing (siCtrl) for four weeks. (*Bhmt*, betaine-homocysteine S-methyltransferase; *Cbs*, cysthationine-beta synthase; *Cth*, cysthathionine gamma-lyase; *Gclc*, glutamate-cysteine ligase, catalytic subunit; *Gclm*, glutamate-cysteine ligase, modifier subunit; *Gls1*, glutaminase 1; *Gnmt*, glycine N-methyltransferase; *Gss*, glutathione synthetase; *Mat1a,* methionine adenosyltransferase 1A; *Mat2a,* methionine adenosyltransferase 2A; *Mat2b,* methionine adenosyltransferase 2B; *Ms*, methionine synthetase; *Mthfr*, methylenetetrahydrofolate reductase; *Mthfs*, synthetase; *Sahh*, S-adenosyl-homocysteinase.) (DMG, dimethyglycine; MTHF, L-methylfolate; SAMe, S-adenosylmethionine; SAH, S-adenosylhomocysteine; THF, tetrahydrofolate.)

(B) Differential expression of mRNA levels from genes significantly different involved in phospholipid biosynthesis in mice on a 0.1% MCDD with si*Gls1* versus siCtrl for four weeks. (*Cept1*, choline/ethanolamine phosphotransferase 1; *Chk*, choline kinase; *Chpt1*, choline phosphotransferase 1; *Etnk2*, ethanolamine kinase 2; *Pcyt1A*, phosphate cytidylyltransferase 1, choline; *Pcyt2*, phosphate cytidylyltransferase 2, ethanolamine; *Pemt*, phosphatidylethanolamine methyltransferase; *Pisd*, phosphatidylserine decarboxylase; *Ptdss1*, phosphatidylserine synthase 1; *Ptdss2*, phosphatidylserine synthase 2.) At least n = 5 were used for each experimental group. Student's t test was used to compare the two groups, and significance was set to p < 0.05 (see also Table S3).

Figure 7. Flowchart of Glutaminase 1 (GLS1)-Inhibition Resolution of Non-alcoholic Steatohepatitis

Deprivation of methionine and choline induces NASH through the inhibition of very-low-density lipoprotein (VLDL) assembly and export. Under these circumstances, excessive glutamine catabolism mediated by GLS1 in NASH accounts for increased levels of glutamate that can be further deaminated to α-ketoglutarate in order to sustain augmented tricarboxylic acids (TCA) cycle anaplerosis and augmented fatty acid oxidation (FAO). Hepatic anaplerotic pathways are energetically backed by elevated oxidative metabolism in the liver through oxidative phosphorylation (OXPHOS). On the other hand, GLS1 inhibition under methionine and choline deprivation is associated with decreased TCA cycle activity, associated diminishment of mitochondrial OXPHOS, and reduced production of reactive oxygen species (ROS). Under these circumstances, serine demand for glutathione (GSH) synthesis is diminished and in alternative serine is channeled to phophatidylcholine synthesis, leading to the formation of lipid-enriched VLDL particles and decreased liver steatosis in a metabolic reprogramming where folates and methionine cycles are relevant. Overall, GLS1 inhibition is suggested as a novel therapeutic approach during NASH management.

known to occur in culture. Moreover, herein, we show that GLS1 silencing is beneficial in animal models of choline and methionine deprivation induced NASH, where NASH is attained as soon as after 4–6 weeks of dietary intervention. In our perspective, it will be important to validate these findings in other dietary models of NASH, specifically in chronic pre-clinical models of NASH, in which timely disease progression resembles more to human pathology. This would be useful to assess efficacy and possible associated side effects of hepatic GLS1 silencing in NASH.

STAR★METHODS

Detailed methods are provided in the online version of this paper and include the following:

- KEY RESOURCES TABLE
- LEAD CONTACT AND MATERIALS AVAILABILITY
- EXPERIMENTAL MODEL AND SUBJECT DETAILS
  - ○ Human Subjects
  - ○ Animal Maintenance
  - ○ Isolation and Culture of Primary Hepatocytes, Hepatic Stellate Cells (HSC) and Kupffer Cells (KC)
  - ○ THLE-2 Cell Line
- METHOD DETAILS
  - ○ Treatments to Primary Mouse Hepatocytes and THLE-2 Cells
  - ○ Treatments to Primary HSC and KC
  - ○ RNA Isolation and Quantitative Real-Time Polymerase Chain Reaction
  - ○ Protein Isolation and Western Blotting

- ○ BODIPY Staining in Isolated Mouse Hepatocytes
- ○ Quantification of Hepatic Lipids
- ○ Determination of Cellular Reactive Oxygen Species (ROS)
- ○ Determination of Mitochondrial Reactive Oxygen Species (ROS)
- ○ Lipid Peroxidation Assay Kit
- ○ Hepatic Fatty Acid Oxidation (FAO)
- ○ Respiration Studies in Liver Mitochondria
- ○ Glutaminase Activity
- ○ Tricarboxylic Acid (TCA) Cycle Activity
- ○ Incorporation of $^{13}C_6$-glucose in Ptd-Cho in Isolated Mouse Hepatocytes
- ○ LCMS Sample Preparation
- ○ Liquid Chromatography and Mass Spectrometry Methods
- ○ LCMS Data Analysis
- ● QUANTIFICATION AND STATISTICAL ANALYSIS
- ● DATA AND CODE AVAILABILITY

SUPPLEMENTAL INFORMATION

Supplemental Information can be found online at https://doi.org/10.1016/j.cmet.2020.01.013.

AUTHOR CONTRIBUTIONS

Conceptualization, J.S., T.C.D., and M.L.M.-C.; Funding Acquisition, M.V.-R., S.C.L., J.M.M., P.A., T.C.D., and M.L.M.-C.; Investigation: J.S., M.N.-G., P.F.-T., L.B.-T., D.F.-R., B.G.-S., X.B., F.L.-O., N.G.-U., M.S.-M., R.R.-A., M.B.-U., I.Z.-F., V.G.-d.J., D.C., C.A., P.I., M.R.-G., S.L., A.C., R.N., M.V.-R., J.M.F.-P., E.V., J.C., P.A., and T.C.D.; Supervision, T.C.D. and M.L.M.-C.; Writing – Original Draft, Review, and Editing, J.S., T.C.D., and M.L.M.-C.

REFERENCES

Alberghina, L., and Gaglio, D. (2014). Redox control of glutamine utilization in cancer. Cell Death Dis. *5*, e1561.

Alonso, C., Fernández-Ramos, D., Varela-Rey, M., Martínez-Arranz, I., Navasa, N., Van Liempd, S.M., Lavín Trueba, J.L., Mayo, R., Ilisso, C.P., de Juan, V.G., et al. (2017). Metabolomic Identification of Subtypes of Nonalcoholic Steatohepatitis. Gastroenterology *152*, 1449–1461.e7.

Ascha, M.S., Hanouneh, I.A., Lopez, R., Tamimi, T.A., Feldstein, A.F., and Zein, N.N. (2010). The incidence and risk factors of hepatocellular carcinoma in patients with nonalcoholic steatohepatitis. Hepatology *51*, 1972–1978.

Barr, J., Caballería, J., Martínez-Arranz, I., Domínguez-Díez, A., Alonso, C., Muntané, J., Pérez-Cormenzana, M., García-Monzón, C., Mayo, R., Martín-Duce, A., et al. (2012). Obesity-dependent metabolic signatures associated with nonalcoholic fatty liver disease progression. J. Proteome Res. *11*, 2521–2532.

Brunelli, L., Caiola, E., Marabese, M., Broggini, M., and Pastorelli, R. (2014). Capturing the metabolomic diversity of KRAS mutants in non-small-cell lung cancer cells. Oncotarget *5*, 4722–4731.

Caballero, F., Fernández, A., Matías, N., Martínez, L., Fucho, R., Elena, M., Caballeria, J., Morales, A., Fernández-Checa, J.C., and García-Ruiz, C. (2010). Specific contribution of methionine and choline in nutritional nonalcoholic steatohepatitis: impact on mitochondrial S-adenosyl-L-methionine and glutathione. J. Biol. Chem. *285*, 18528–18536.

Canbay, A., and Sowa, J.P. (2019). L-Ornithine L-Aspartate (LOLA) as a Novel Approach for Therapy of Non-alcoholic Fatty Liver Disease. Drugs *79* (*Suppl 1*), 39–44.

Cano, A., Buqué, X., Martínez-Uña, M., Aurrekoetxea, I., Menor, A., García-Rodríguez, J.L., Lu, S.C., Martínez-Chantar, M.L., Mato, J.M., Ochoa, B., and Aspichueta, P. (2011). Methionine adenosyltransferase 1A gene deletion disrupts hepatic very low-density lipoprotein assembly in mice. Hepatology *54*, 1975–1986.

Cassago, A., Ferreira, A.P., Ferreira, I.M., Fornezari, C., Gomes, E.R., Greene, K.S., Pereira, H.M., Garratt, R.C., Dias, S.M., and Ambrosio, A.L. (2012). Mitochondrial localization and structure-based phosphate activation mechanism of Glutaminase C with implications for cancer metabolism. Proc. Natl. Acad. Sci. USA *109*, 1092–1097.

Cassidy, S., and Syed, B.A. (2016). Nonalcoholic steatohepatitis (NASH) drugs market. Nat. Rev. Drug Discov. *15*, 745–746.

Cefalù, A.B., Pirruccello, J.P., Noto, D., Gabriel, S., Valenti, V., Gupta, N., Spina, R., Tarugi, P., Kathiresan, S., and Averna, M.R. (2013). A novel APOB mutation identified by exome sequencing cosegregates with steatosis, liver cancer, and hypocholesterolemia. Arterioscler. Thromb. Vasc. Biol. *33*, 2021–2025.

Chen, N.C., Yang, F., Capecci, L.M., Gu, Z., Schafer, A.I., Durante, W., Yang, X.F., and Wang, H. (2010). Regulation of homocysteine metabolism and methylation in human and mouse tissues. FASEB J. *24*, 2804–2817.

Cole, L.K., Vance, J.E., and Vance, D.E. (2012). Phosphatidylcholine biosynthesis and lipoprotein metabolism. Biochim. Biophys. Acta *1821*, 754–761.

Dasarathy, S., Kasumov, T., Edmison, J.M., Gruca, L.L., Bennett, C., Duenas, C., Marczewski, S., McCullough, A.J., Hanson, R.W., and Kalhan, S.C. (2009). Glycine and urea kinetics in nonalcoholic steatohepatitis in human: effect of intralipid infusion. Am. J. Physiol. Gastrointest. Liver Physiol. *297*, G567–G575.

De Chiara, F., Heebøll, S., Marrone, G., Montoliu, C., Hamilton-Dutoit, S., Ferrandez, A., Andreola, F., Rombouts, K., Grønbæk, H., Felipo, V., et al. (2018). Urea cycle dysregulation in non-alcoholic fatty liver disease. J. Hepatol. *69*, 905–915.

De Chiara, F., Thomsen, K.L., Habtesion, A., Jones, H., Davies, N., Gracia-Sancho, J., Manicardi, N., Hall, A., Andreola, F., Paish, H.L., et al. (2019). Ammonia Scavenging Prevents Progression of Fibrosis in Experimental Nonalcoholic Fatty Liver Disease. Hepatology.

DeLaBarre, B., Gross, S., Fang, C., Gao, Y., Jha, A., Jiang, F., Song J, J., Wei, W., and Hurov, J.B. (2011). Full-length human glutaminase in complex with an allosteric inhibitor. Biochemistry *50*, 10764–10770.

Di Filippo, M., Moulin, P., Roy, P., Samson-Bouma, M.E., Collardeau-Frachon, S., Chebel-Dumont, S., Peretti, N., Dumortier, J., Zoulim, F., Fontanges, T., et al. (2014). Homozygous MTTP and APOB mutations may lead to hepatic steatosis and fibrosis despite metabolic differences in congenital hypocholesterolemia. J. Hepatol. *61*, 891–902.

Díaz-Herrero, M.M., del Campo, J.A., Carbonero-Aguilar, P., Vega-Pérez, J.M., Iglesias-Guerra, F., Periñán, I., Miñano, F.J., Bautista, J., and Romero-Gómez, M. (2014). THDP17 decreases ammonia production through glutaminase inhibition. A new drug for hepatic encephalopathy therapy. PLoS ONE *9*, e109787.

Du, K., Hyun, J., Premont, R.T., Choi, S.S., Michelotti, G.A., Swiderska-Syn, M., Dalton, G.D., Thelen, E., Rizi, B.S., Jung, Y., et al. (2018). Hedgehog-YAP Signaling Pathway Regulates Glutaminolysis to Control Activation of Hepatic Stellate Cells. Gastroenterology *154*, 1465–1479.e1413.

Eisenberg, S., and Olivecrona, T. (1979). Very low density lipoprotein. Fate of phospholipids, cholesterol, and apolipoprotein C during lipolysis in vitro. J. Lipid Res. *20*, 614–623.

Elgogary, A., Xu, Q., Poore, B., Alt, J., Zimmermann, S.C., Zhao, L., Fu, J., Chen, B., Xia, S., Liu, Y., et al. (2016). Combination therapy with BPTES nanoparticles and metformin targets the metabolic heterogeneity of pancreatic cancer. Proc. Natl. Acad. Sci. USA *113*, E5328–E5336.

Elizalde, M., Urtasun, R., Azkona, M., Latasa, M.U., Goñi, S., García-Irigoyen, O., Uriarte, I., Segura, V., Collantes, M., Di Scala, M., et al. (2014). Splicing regulator SLU7 is essential for maintaining liver homeostasis. J. Clin. Invest. *124*, 2909–2920.

Embade, N., Fernández-Ramos, D., Varela-Rey, M., Beraza, N., Sini, M., Gutiérrez de Juan, V., Woodhoo, A., Martínez-López, N., Rodríguez-Iruretagoyena, B., Bustamante, F.J., et al. (2012). Murine double minute 2 regulates Hu antigen R stability in human liver and colon cancer through NEDDylation. Hepatology *55*, 1237–1248.

Faubert, B., Vincent, E.E., Griss, T., Samborska, B., Izreig, S., Svensson, R.U., Mamer, O.A., Avizonis, D., Shackelford, D.B., Shaw, R.J., and Jones, R.G. (2014). Loss of the tumor suppressor LKB1 promotes metabolic reprogramming of cancer cells via HIF-1α. Proc. Natl. Acad. Sci. USA *111*, 2554–2559.

Felig, P., Wahren, J., Hendler, R., and Brundin, T. (1974). Splanchnic glucose and amino acid metabolism in obesity. J. Clin. Invest. *53*, 582–590.

Folch, J., Lees, M., and Sloane Stanley, G.H. (1957). A simple method for the isolation and purification of total lipides from animal tissues. J. Biol. Chem. *226*, 497–509.

Frades, I., Andreasson, E., Mato, J.M., Alexandersson, E., Matthiesen, R., and Martínez-Chantar, M.L. (2015). Integrative genomic signatures of hepatocellular carcinoma derived from nonalcoholic Fatty liver disease. PLoS ONE *10*, e0124544.

Fujita, K., Nozaki, Y., Wada, K., Yoneda, M., Fujimoto, Y., Fujitake, M., Endo, H., Takahashi, H., Inamori, M., Kobayashi, N., et al. (2009). Dysfunctional very-low-density lipoprotein synthesis and release is a key factor in nonalcoholic steatohepatitis pathogenesis. Hepatology *50*, 772–780.

Gao, P., Tchernyshyov, I., Chang, T.C., Lee, Y.S., Kita, K., Ochi, T., Zeller, K.I., De Marzo, A.M., Van Eyk, J.E., Mendell, J.T., and Dang, C.V. (2009). c-Myc suppression of miR-23a/b enhances mitochondrial glutaminase expression and glutamine metabolism. Nature *458*, 762–765.

Gao, X., van der Veen, J.N., Hermansson, M., Ordoñez, M., Gomez-Muñoz, A., Vance, D.E., and Jacobs, R.L. (2015). Decreased lipogenesis in white adipose

tissue contributes to the resistance to high fat diet-induced obesity in phosphatidylethanolamine N-methyltransferase-deficient mice. Biochim. Biophys. Acta *1851*, 152–162.

Gross, M.I., Demo, S.D., Dennison, J.B., Chen, L., Chernov-Rogan, T., Goyal, B., Janes, J.R., Laidig, G.J., Lewis, E.R., Li, J., et al. (2014). Antitumor activity of the glutaminase inhibitor CB-839 in triple-negative breast cancer. Mol. Cancer Ther. *13*, 890–901.

Gutiérrez-de-Juan, V., López de Davalillo, S., Fernández-Ramos, D., Barbier-Torres, L., Zubiete-Franco, I., Fernández-Tussy, P., Simon, J., Lopitz-Otsoa, F., de Las Heras, J., Iruzubieta, P., et al. (2017). A morphological method for ammonia detection in liver. PLoS ONE *12*, e0173914.

Hirschey, M.D., Shimazu, T., Goetzman, E., Jing, E., Schwer, B., Lombard, D.B., Grueter, C.A., Harris, C., Biddinger, S., Ilkayeva, O.R., et al. (2010). SIRT3 regulates mitochondrial fatty-acid oxidation by reversible enzyme deacetylation. Nature *464*, 121–125.

Huang, Q., Stalnecker, C., Zhang, C., McDermott, L.A., Iyer, P., O'Neill, J., Reimer, S., Cerione, R.A., and Katt, W.P. (2018). Characterization of the interactions of potent allosteric inhibitors with glutaminase C, a key enzyme in cancer cell glutamine metabolism. J. Biol. Chem. *293*, 3535–3545.

Hyötyläinen, T., Jerby, L., Petäjä, E.M., Mattila, I., Jäntti, S., Auvinen, P., Gastaldelli, A., Yki-Järvinen, H., Ruppin, E., and Orešič, M. (2016). Genome-scale study reveals reduced metabolic adaptability in patients with non-alcoholic fatty liver disease. Nat. Commun. *7*, 8994.

Iozzo, P., Bucci, M., Roivainen, A., Nagren, K., Jarvisalo, M.J., Kiss, J., Guiducci, L., Fielding, B., Naum, A.G., Borra, R., et al. (2010). Fatty acid metabolism in the liver, measured by positron emission tomography, is increased in obese individuals. Gastroenterology *139*, 846–856, 856.e1–e6.

Iruarrizaga-Lejarreta, M., Varela-Rey, M., Fernández-Ramos, D., Martínez-Arranz, I., Delgado, T.C., Simon, J., Juan, V.G., delaCruz-Villar, L., Azkargorta, M., Lavin, J.L., et al. (2017). Role of Aramchol in steatohepatitis and fibrosis in mice. Hepatol Commun *1*, 911–927.

Jalan, R., Wright, G., Davies, N.A., and Hodges, S.J. (2007). L-Ornithine phenylacetate (OP): a novel treatment for hyperammonemia and hepatic encephalopathy. Med. Hypotheses *69*, 1064–1069.

Karpe, F., Olivecrona, T., Olivecrona, G., Samra, J.S., Summers, L.K., Humphreys, S.M., and Frayn, K.N. (1998). Lipoprotein lipase transport in plasma: role of muscle and adipose tissues in regulation of plasma lipoprotein lipase concentrations. J. Lipid Res. *39*, 2387–2393.

Koliaki, C., Szendroedi, J., Kaul, K., Jelenik, T., Nowotny, P., Jankowiak, F., Herder, C., Carstensen, M., Krausch, M., Knoefel, W.T., et al. (2015). Adaptation of hepatic mitochondrial function in humans with non-alcoholic fatty liver is lost in steatohepatitis. Cell Metab. *21*, 739–746.

Kuge, O., and Nishijima, M. (1997). Phosphatidylserine synthase I and II of mammalian cells. Biochim. Biophys. Acta *1348*, 151–156.

Kuge, O., Saito, K., and Nishijima, M. (1997). Cloning of a Chinese hamster ovary (CHO) cDNA encoding phosphatidylserine synthase (PSS) II, overexpression of which suppresses the phosphatidylserine biosynthetic defect of a PSS I-lacking mutant of CHO-K1 cells. J. Biol. Chem. *272*, 19133–19139.

Leclercq, I.A., Lebrun, V.A., Stärkel, P., and Horsmans, Y.J. (2007). Intrahepatic insulin resistance in a murine model of steatohepatitis: effect of PPARgamma agonist pioglitazone. Lab. Invest. *87*, 56–65.

Li, H., Wang, L., Yan, X., Liu, Q., Yu, C., Wei, H., Li, Y., Zhang, X., He, F., and Jiang, Y. (2011). A proton nuclear magnetic resonance metabonomics approach for biomarker discovery in nonalcoholic fatty liver disease. J. Proteome Res. *10*, 2797–2806.

Li, B., Cao, Y., Meng, G., Qian, L., Xu, T., Yan, C., Luo, O., Wang, S., Wei, J., Ding, Y., et al. (2018). Targeting glutaminase 1 attenuates stemness properties in hepatocellular carcinoma by increasing reactive oxygen species and suppressing Wnt/beta-catenin pathway. EBioMedicine.

Maddocks, O.D., Labuschagne, C.F., Adams, P.D., and Vousden, K.H. (2016). Serine Metabolism Supports the Methionine Cycle and DNA/RNA Methylation through De Novo ATP Synthesis in Cancer Cells. Mol. Cell *61*, 210–221.

Maldonado, E.N., Delgado, I., Furland, N.E., Buqué, X., Iglesias, A., Aveldaño, M.I., Zubiaga, A., Fresnedo, O., and Ochoa, B. (2014). The E2F2 transcription

factor sustains hepatic glycerophospholipid homeostasis in mice. PLoS ONE *9*, e112620.

Matés, J.M., Segura, J.A., Martín-Rufián, M., Campos-Sandoval, J.A., Alonso, F.J., and Márquez, J. (2013). Glutaminase isoenzymes as key regulators in metabolic and oxidative stress against cancer. Curr. Mol. Med. *13*, 514–534.

Mato, J.M., Martínez-Chantar, M.L., and Lu, S.C. (2013). S-adenosylmethionine metabolism and liver disease. Ann. Hepatol. *12*, 183–189.

Millar, J.S., Cromley, D.A., McCoy, M.G., Rader, D.J., and Billheimer, J.T. (2005). Determining hepatic triglyceride production in mice: comparison of poloxamer 407 with Triton WR-1339. J. Lipid Res. *46*, 2023–2028.

Miller, R.A., Shi, Y., Lu, W., Pirman, D.A., Jatkar, A., Blatnik, M., Wu, H., Cárdenas, C., Wan, M., Foskett, J.K., et al. (2018). Targeting hepatic glutaminase activity to ameliorate hyperglycemia. Nat. Med. *24*, 518–524.

Noga, A.A., Zhao, Y., and Vance, D.E. (2002). An unexpected requirement for phosphatidylethanolamine N-methyltransferase in the secretion of very low density lipoproteins. J. Biol. Chem. *277*, 42358–42365.

Nossen, J.O., Rustan, A.C., Gloppestad, S.H., Målbakken, S., and Drevon, C.A. (1986). Eicosapentaenoic acid inhibits synthesis and secretion of triacylglycerols by cultured rat hepatocytes. Biochim. Biophys. Acta *879*, 56–65.

Pitman, J.L., Bonnet, D.J., Curtiss, L.K., and Gekakis, N. (2011). Reduced cholesterol and triglycerides in mice with a mutation in Mia2, a liver protein that localizes to ER exit sites. J. Lipid Res. *52*, 1775–1786.

Porteiro, B., Fondevila, M.F., Delgado, T.C., Iglesias, C., Imbernon, M., Iruzubieta, P., Crespo, J., Zabala-Letona, A., Fernø, J., González-Terán, B., et al. (2017). Hepatic p63 regulates steatosis via IKKβ/ER stress. Nat. Commun. *8*, 15111.

Rahman, A., Smith, F.P., Luc, P.T., and Woolley, P.V. (1985). Phase I study and clinical pharmacology of 6-diazo-5-oxo-L-norleucine (DON). Invest. New Drugs *3*, 369–374.

Rahman, S.M., Qadri, I., Janssen, R.C., and Friedman, J.E. (2009). Fenofibrate and PBA prevent fatty acid-induced loss of adiponectin receptor and pAMPK in human hepatoma cells and in hepatitis C virus-induced steatosis. J. Lipid Res. *50*, 2193–2202.

Rizki, G., Arnaboldi, L., Gabrielli, B., Yan, J., Lee, G.S., Ng, R.K., Turner, S.M., Badger, T.M., Pitas, R.E., and Maher, J.J. (2006). Mice fed a lipogenic methionine-choline-deficient diet develop hypermetabolism coincident with hepatic suppression of SCD-1. J. Lipid Res. *47*, 2280–2290.

Romestaing, C., Piquet, M.A., Letexier, D., Rey, B., Mourier, A., Servais, S., Belouze, M., Rouleau, V., Dautresme, M., Ollivier, I., et al. (2008). Mitochondrial adaptations to steatohepatitis induced by a methionine- and choline-deficient diet. Am. J. Physiol. Endocrinol. Metab. *294*, E110–E119.

Rosca, M.G., Vazquez, E.J., Chen, Q., Kerner, J., Kern, T.S., and Hoppel, C.L. (2012). Oxidation of fatty acids is the source of increased mitochondrial reactive oxygen species production in kidney cortical tubules in early diabetes. Diabetes *61*, 2074–2083.

Ruiz, J.I., and Ochoa, B. (1997). Quantification in the subnanomolar range of phospholipids and neutral lipids by monodimensional thin-layer chromatography and image analysis. J. Lipid Res. *38*, 1482–1489.

Sahai, A., Pan, X., Paul, R., Malladi, P., Kohli, R., and Whitington, P.F. (2006). Roles of phosphatidylinositol 3-kinase and osteopontin in steatosis and aminotransferase release by hepatocytes treated with methionine-choline-deficient medium. Am. J. Physiol. Gastrointest. Liver Physiol. *291*, G55–G62.

Sappington, D.R., Siegel, E.R., Hiatt, G., Desai, A., Penney, R.B., Jamshidi-Parsian, A., Griffin, R.J., and Boysen, G. (2016). Glutamine drives glutathione synthesis and contributes to radiation sensitivity of A549 and H460 lung cancer cell lines. Biochim. Biophys. Acta *1860*, 836–843.

Satapati, S., Kucejova, B., Duarte, J.A., Fletcher, J.A., Reynolds, L., Sunny, N.E., He, T., Nair, L.A., Livingston, K.A., Fu, X., et al. (2015). Mitochondrial metabolism mediates oxidative stress and inflammation in fatty liver. J. Clin. Invest. *125*, 4447–4462.

Sellmann, C., Jin, C.J., Degen, C., De Bandt, J.P., and Bergheim, I. (2015). Oral Glutamine Supplementation Protects Female Mice from Nonalcoholic Steatohepatitis. J. Nutr. *145*, 2280–2286.

Shukla, K., Ferraris, D.V., Thomas, A.G., Stathis, M., Duvall, B., Delahanty, G., Alt, J., Rais, R., Rojas, C., Gao, P., et al. (2012). Design, synthesis, and pharmacological evaluation of bis-2-(5-phenylacetamido-1,2,4-thiadiazol-2-yl) ethyl sulfide 3 (BPTES) analogs as glutaminase inhibitors. J. Med. Chem. *55*, 10551–10563.

Sirtori, C.R., Pavanello, C., and Bertolini, S. (2014). Microsomal transfer protein (MTP) inhibition-a novel approach to the treatment of homozygous hypercholesterolemia. Ann. Med. *46*, 464–474.

Söderberg, C., Stål, P., Askling, J., Glaumann, H., Lindberg, G., Marmur, J., and Hultcrantz, R. (2010). Decreased survival of subjects with elevated liver function tests during a 28-year follow-up. Hepatology *51*, 595–602.

Sunny, N.E., Parks, E.J., Browning, J.D., and Burgess, S.C. (2011). Excessive hepatic mitochondrial TCA cycle and gluconeogenesis in humans with nonalcoholic fatty liver disease. Cell Metab. *14*, 804–810.

Thangavelu, K., Pan, C.Q., Karlberg, T., Balaji, G., Uttamchandani, M., Suresh, V., Schüler, H., Low, B.C., and Sivaraman, J. (2012). Structural basis for the allosteric inhibitory mechanism of human kidney-type glutaminase (KGA) and its regulation by Raf-Mek-Erk signaling in cancer cell metabolism. Proc. Natl. Acad. Sci. USA *109*, 7705–7710.

Thomas, A.G., Rojas, C., Tanega, C., Shen, M., Simeonov, A., Boxer, M.B., Auld, D.S., Ferraris, D.V., Tsukamoto, T., and Slusher, B.S. (2013). Kinetic characterization of ebselen, chelerythrine and apomorphine as glutaminase inhibitors. Biochem. Biophys. Res. Commun. *438*, 243–248.

van de Wier, B., Balk, J.M., Haenen, G.R., Giamouridis, D., Bakker, J.A., Bast, B.C., den Hartog, G.J., Koek, G.H., and Bast, A. (2013). Elevated citrate levels in non-alcoholic fatty liver disease: the potential of citrate to promote radical production. FEBS Lett. *587*, 2461–2466.

Wang, J.B., Erickson, J.W., Fuji, R., Ramachandran, S., Gao, P., Dinavahi, R., Wilson, K.F., Ambrosio, A.L., Dias, S.M., Dang, C.V., and Cerione, R.A. (2010). Targeting mitochondrial glutaminase activity inhibits oncogenic transformation. Cancer Cell *18*, 207–219.

Wolf, M.J., Adili, A., Piotrowitz, K., Abdullah, Z., Boege, Y., Stemmer, K., Ringelhan, M., Simonavicius, N., Egger, M., Wohlleber, D., et al. (2014). Metabolic activation of intrahepatic CD8+ T cells and NKT cells causes nonalcoholic steatohepatitis and liver cancer via cross-talk with hepatocytes. Cancer Cell *26*, 549–564.

Younossi, Z.M., Koenig, A.B., Abdelatif, D., Fazel, Y., Henry, L., and Wymer, M. (2016). Global epidemiology of nonalcoholic fatty liver disease-Meta-analytic assessment of prevalence, incidence, and outcomes. Hepatology *64*, 73–84.

Yu, D., Shi, X., Meng, G., Chen, J., Yan, C., Jiang, Y., Wei, J., and Ding, Y. (2015). Kidney-type glutaminase (GLS1) is a biomarker for pathologic diagnosis and prognosis of hepatocellular carcinoma. Oncotarget *6*, 7619–7631.

Yuan, L., Sheng, X., Clark, L.H., Zhang, L., Guo, H., Jones, H.M., Willson, A.K., Gehrig, P.A., Zhou, C., and Bae-Jump, V.L. (2016). Glutaminase inhibitor compound 968 inhibits cell proliferation and sensitizes paclitaxel in ovarian cancer. Am. J. Transl. Res. *8*, 4265–4277.

Yuneva, M.O., Fan, T.W., Allen, T.D., Higashi, R.M., Ferraris, D.V., Tsukamoto, T., Matés, J.M., Alonso, F.J., Wang, C., Seo, Y., et al. (2012). The metabolic profile of tumors depends on both the responsible genetic lesion and tissue type. Cell Metab. *15*, 157–170.

Zhao, Y., Su, B., Jacobs, R.L., Kennedy, B., Francis, G.A., Waddington, E., Brosnan, J.T., Vance, J.E., and Vance, D.E. (2009). Lack of phosphatidylethanolamine N-methyltransferase alters plasma VLDL phospholipids and attenuates atherosclerosis in mice. Arterioscler. Thromb. Vasc. Biol. *29*, 1349–1355.

Zubiete-Franco, I., Fernández-Tussy, P., Barbier-Torres, L., Simon, J., Fernández-Ramos, D., Lopitz-Otsoa, F., Gutiérrez-de Juan, V., de Davalillo, S.L., Duce, A.M., Iruzubieta, P., et al. (2017). Deregulated neddylation in liver fibrosis. Hepatology *65*, 694–709.

STAR★METHODS

KEY RESOURCES TABLE

REAGENT or RESOURCE	SOURCE	IDENTIFIER
Antibodies		
Albumin antibody	Affinity Biologicals	#CatPA1-25673; RRID:AB_2539935
Anti-Apolipoprotein B antibody	Millipore	#CatAB742; RRID:AB_92217
GAPDH antibody [6C5]	Abcam	#CatAb8245; RRID:AB_2107448
Anti-GLS1	Agios Pharmaceuticals	N/A
Anti-GLS2 antibody	LifeSpan Biosciences	#CatLS-C80586-100; RRID: AB_1594624
Glutamine Synthetase Antibody	Novus Biologicals	#CatNB110-41404; RRID:AB_790020
Mouse Anti-Human HNF4 alpha Monoclonal Antibody, Unconjugated, Clone K9218	Actif SCETI (Perseus Proteomics)	Cat# PP-K9218-00 RRID:AB_1964277
Anti-mouse IgG, HRP-linked Antibody	Cell Signaling	#Cat7076S RRID:AB_330924
Anti-rabbit IgG, HRP-linked Antibody	Cell Signaling	#Cat7074S; RRID:AB_2099233
Rat anti-mouse F4/80:ANTIGEN Monoclonal antibody, Biotin Conjugated, Clone CI:A3-1	Abd Serotec	#CatMCA497-BB; RRID:AB_323893
Cy3-AffiniPure Goat Anti-Rabbit IgG (H+L) antibody	Jackson ImmunoResearch	#Cat111-165-003; RRID:AB_2338000
Goat anti-chicken-Alexa fluor488	Abcam	Cat# ab150169; RRID:AB_2636803
Fluorescein (FITC)-AffiniPure Goat Anti-Rabbit IgG (H+L) antibody	Jackson ImmunoResearch	#Cat111-095-003; RRID:AB_2337972
Biological Samples		
cDNA of NASH patients	Supplied by MD PhD Javier Crespo García	Hospital Universitario Marqués de Valdecilla www.humv.es
Serum of NASH patients	Already published study	Barr et al., 2012https://doi.org/10.1021/pr201223p
Paraffin-embedded liver NASH patients	Supplied by MD PhD Erica Villa	Azienda Ospedaliero-Universitaria http://www.ao-pisa.toscana.it/
Chemicals, Peptides, and Recombinant Proteins		
2-propanol	Sigma-Aldrich	#Cat 19516 CAS 67-63-0
30% Acrilamide/Bis Solution	Bio-Rad	#Cat161-0156
Acetonitrile	Pierce	#Cat51101
Ac-DEVD-AFC Caspase-3- substrate	Enzo	ALX-260-032
Adenosine 5′- diphosphate sodium salt	Sigma-Aldrich	A2754CAS 20398-34-9
Agarose	Sigma-Aldrich	A9539 CAS 9012-36-6
Bis-2(5-phenylacetamido-1,3,4-thiadiazol-2-yl)ethyl sulfide (BPTES)	Sigma-Aldrich	SML0601-25MG CAS 314045-39-1
Bore-dipyromethene (BODIPY)	Molecular Probes (ThermoFischer)	D3922
CHAPS	Sigma-Aldrich	CHAPS-RO
Chloroform	Sigma-Aldrich	C2431CAS 67-66-1
Corning® Collagen I, Rat Tail, 100 mg	Corning	#Cat354236
Collagenase type IV, CLS-4	Worthington	LS004188
Dako EnVIsion system, Peroxidase	Dako	K5007

(Continued on next page)

Continued

REAGENT or RESOURCE	SOURCE	IDENTIFIER
2-(4-Amidinophenyl)-6-indolecarbamidine dihydrochloride, 4′,6-Diamidino-2-phenylindole dihydrochlorid (DAPI)	Sigma-Aldrich	D9542 CAS 28718-90-3
DharmaFECT 1 Transfection Reagent	Dharmacon	T-2001-01
Direct Red 80	Sigma-Aldrich	365548-25G CAS 2610-10-8
DMEM/F-12 methionine and choline-deficient media	GIBCO (ThermoFischer)	ME120128L1EDC11632701
DPX	Sigma-Aldrich	#Cat06522
DTT	Sigma-Aldrich	DTT-RO
EDTA	Sigma-Aldrich	E9884
EnVision+ System HRP	Dako	K4001
Eosin B	Sigma-Aldrich	#Cat2853
Fast Green FCF	Sigma-Aldrich	F7258-25GCAS 2353-45-9
Carbonyl cyanide-p-trifluoromethoxyphenylhydrazone (FCCP)	CaymanChem	#Cat15218CAS 370-86-5
caspase-3 (human),	Enzo Life Sciences	ALX-201059
Fetal Bovine Serum	GIBCO (ThermoFischer)	A38401
Formic Acid	PanReac AppliChem	#Cat1002641000
Glucose [U-^{13}C]	Sigma-Aldrich	#Cat389374 CAS 110187-42-3
Glutamine [U-^{13}C] 99%	Cambridge Isotope Laboratoires	CLM-1822CAS 184161-19-1
Harris Hematoxylin	Bio-Optica	#Cat05-06005/L
Histo-Clear	Electron Microscopy Sciences	#Cat64110-004
Hydrogen Peroxide 30% w/v	PanReac AppliChem	#Cat121076 CAS 7722-84-1
Invivofectamine^{TM} 3.0 Reagent	ThermoFischer	IVFs3001
Isoflurane	Baxter SL	NR60378
Leukine/encephalin acetate salt hydrate	Sigma-Aldrich	CAS 588-25-6
L-glutamine	GIBCO (ThermoFischer)	#Cat25030-024
Lipopolysaccharide from *Escherichia coli* O111:B4	Sigma-Aldrich	L3012-10MG
Methanol	PanReac AppliChem	#Cat1610911714
Minimum Essential Media	GIBCO (ThermoFischer)	#Cat31095029
Mount Quick Aqueous	Bio-Optica	#Cat05-1740
N-(2,2,2-Trifluoroethyl)-9-[4-[4-[[[4′-(trifluoromethyl)[1,1′-biphenyl]2-yl]carbonyl]amino]-1 piperidinyl]butyl]9H-fluoren-9-carboxamde (Lomitapide)	Sigma-Aldrich	SML1385 CAS 182431-12-5
OCT	Pioneer	PRC/OCT
Oleic acid	Sigma-Aldrich	O1008
Oligomycin	Sigma-Aldrich	O4876-5MG CAS1404-19-9
Oxygen	Air Liquide SLU	ESCG101710
Palmitic acid |1-^{14}C] (56.1 mCi/mmol)	Perkin Elmer	NEC075H
Paraformaldehyde 4% solution in PBS	Santa Cruz	Sc-281692 CAS 30525-89-4
Penicillin-Streptomycin-Glutamine (100x)	GIBCO (ThermoFischer)	#Cat10378016
Percoll® Plus	GE Healthcare (Sigma-Aldrich)	GE17-5445-01
Picric Acid	PanReac AppliChem	#Cat141048-1610CAS 88-89-1
PIPES	Sigma-Aldrich	P6757
Pluronic^{TM} F-127, low UV absorbance (Poloxamer P-407)	Invitrogen (ThermoFischer)	P6867

Continued

REAGENT or RESOURCE	SOURCE	IDENTIFIER
Protease Inhibitor Cocktail Tablets	Roche Diagnostics	#Cat11697498001
Ponceau S Solution	Sigma-Aldrich	P7170-1L CAS 6226-79-5
RPMI-1640	GIBCO (ThermoFischer)	#Cat1185-093
Rotenone	Sigma-Aldrich	R8875 CAS 83-79-4
Sodium chloride	PanReac AppliChem	#Cat1064041000
Sodium dodecyl sulfate	Sigma-Aldrich	L5750 CAS 151-21-3
Sodium orthovanadate	Sigma-Aldrich	S6508-50G
Sodium fluoride	Sigma-Aldrich	S7920-100G
Succinate	Sigma-Aldrich	S9512
Sudan-III	PanReac AppliChem	#Cat251731 CAS 85-86-9
Triton X-100	Sigma-Aldrich	#Cat100-500mL
Tris Base	Fisher	BP152-1
Trizol	Invitrogen (ThermoFischer)	#Cat15596026
XF-Calibrant (pH 7.4)	Seahorse Bioscience	#Cat100840-000
Critical Commercial Assays		
CellROX Deep Green Reagent	ThermoFischer	C104444
DNase I, amplification Grade	Invitrogen (ThermoFischer)	#Cat18068015
Fatty acids Kit	Wako Chemicals	#Cat434-91975
Lipid Peroxidation (MDA) Assay Kit	Sigma-Aldrich	MAK085
M-MLV Reverse Transcriptase (200 U/μL)	Invitrogen (ThermoFischer)	#Cat28025013
MitoSOX™ Red MItochondrial Superoxide Indicator	Invitrogen (ThermoFischer)	M36008
Phospholipid Assay Kit	Sigma-Aldrich	MAK122
SYBR® Select Master Mix	Applied Biosystems (ThermoFischer)	#Cat44720903
Protein Assay Dye Reagent Concentrate (Bradford)	Bio-Rad	#Cat500-0006
Triglyceride Assay Kit	Abcam	ab65336
Vector® VIP Peroxidase Substrate Kit	Vector Laboratories	SK-4600
Experimental Models: Cell Lines		
Human: THLE-2 cells	ATCC®	THLE-2 (ATCC® CRL-2706™)
Experimental Models: Organisms/Strains		
0.1% methionine and choline-deficient diet (0.1% MCDD)	Research Diets	A02082006i
Choline-deficient high-fat diet (CD-HFD)	Research Diets	D05010402
C57BL/6 mouse	Charles River	C57BL/6NCtrl
Teklad Global 14% Protein Rodent Maintenance diet	Envirgo	2014C
Mat1a−/− mouse	CIC bioGUNE animal facility	N/A
Mat1a+/+ mouse	CIC bioGUNE animal facility	N/A
Oligonucleotides		
Gls Ambion® *In vivo* Pre-designed siRNA	Ambion (ThermoFischer)	#Cat4390771 ID: s66756
Silencer™ Negative Control No. 1 siRNA	Ambion (ThermoFischer)	AM4635
siRNA targeting sequence: *Gls1*: Fw 5′- *GCAAUAGGAUAUUACUUAATT*- 3′Rv 5′- *UUAAGUAAUAUCCUAUUGCAA*- 3′	Sigma-Aldrich	N/A
siRNA targeting sequence: Negative Control: Fw 5′- *AAUUCUCCGAACGUGUCACGU[dT][dT]*- 3′Rv 5′- *ACGUGACACGUUCGGAGAAUU [dT][dT]*- 3′	Sigma-Aldrich	N/A

(*Continued on next page*)

REAGENT or RESOURCE	SOURCE	IDENTIFIER
Software and Algorithms		
ImageJ	NIH	https://imagej.nih.gov/ij/index.html RRID SCR_003070
MassLynx MS	Waters Corp	http://www.waters.com/waters/es_ES/MassLynx-Mass-Spectrometry-Software-/nav.htm?cid=513164&locale=es_ES RRID: SCR_014271
QuanLynx Application Manager	Waters Corp	#Cat720001677EN http://www.waters.com/waters/educationInstance.htm?eiid=10137743
Prism 5	Graphad Software	https://www.graphpad.com/ RRID: SCR_00278
DDS Research sample size calculator	DSS Research	https://www.dssresearch.com/resources/calculators/sample-size-calculator-average/
Other		
300SL Liquid Scintillation Counter	LabLogic	N/A
Acquity-SQD UPLC	Waters Corp	N/A
AXIO Imager A1 Manual	Carl Zeiss	N/A
AXIO Imager D1 Upright Fluorescence Microscope	Carl Zeiz	N/A
BD FACSCanto™ II	BD Biosciences	N/A
BEH Amide Collumn	Waters Corp	#Cat186004802
BEH C18 Column	Waters Corp	#Cat186002350
Cryostate	Leica Biossystems	CM 1850 UV
Medical X-Ray Film	Fujifilm	#Cat47410 19289
Nitrocellulose transfer membrane	ThermoFischer	LC2009
Omnican ® 100	Braun	#Cat9151141
Precellys Tissue Homogenizer	Bertin Instruments	N/A
Seahorse XF24-3 Extracellular Flux Analyzer	Seahorse Bioscience (Agilent technologies)	N/A
Selectra Junior® Spinlab 100 analyzer	Vital Scientific	#Cat0200-013-01
Spectramax M2	bioNova	N/A
SpeedVac™	Thermofischer	SPD131DDA
SYNAPT G2 HDMS TOF	Waters Corp	N/A
Thin-layer chromatography (TLC) silica sheets 20x20cm	Merck Millipore	#Cat1055530001
Tissue Homogenizer	FasPrep	N/A
Type 50.4 Ti Fixed-Angle Titanium Rotor	Beckamn Coulter	#Cat377299
ViiA 7 Real-Time PCR System	Applied Biosystems (ThermoFischer)	#Cat4453545
Whatman paper 3MM Chr	GE Healthcare	#Cat3030-931
XF4-3 fluxpak	Seahorse Bioscience (Agilent technologies)	#Cat102070-001

LEAD CONTACT AND MATERIALS AVAILABILITY

Further information and requests for resources and reagents should be directed to and will be fulfilled by the Lead Contact, María Luz Martínez-Chantar (mlmartinez@cicbiogune.es). This study did not generate new unique reagents.

EXPERIMENTAL MODEL AND SUBJECT DETAILS

Human Subjects

The work described has been carried out in accordance with the code of ethics of the World Medical Association (Declaration of Helsinki) for experiments involving humans after obtaining informed consent. A total of 221 patients, from a study previously published

elsewhere (Barr et al., 2012) were used. Inclusion criteria included (1) age 18–75 years; (2) no known acute or chronic disease except for obesity or type 2 diabetes based on medical history, physical examination, and standard laboratory tests; (3) alcohol consumption was less than 20 g/day for women and 30 g/day for men; (4) 76% of the patients (Control and NASH) were women. Exclusion criteria included viral- and drug-induced causes of liver disease. All of the subjects were of Caucasian origin. The institutional review board at each of the participating hospitals approved the study and written informed consent was obtained from all patients. For all the patients, diagnoses were established histologically in liver biopsy specimens. Following assessment, patients were classified by the pathologists into two histological groups: (1) Normal liver and (2) NASH (presence as determined by the pathologist). For all the subjects, blood was drawn on the morning a liver biopsy was performed, following a minimum 8 h, overnight fast. Serum was separated and stored at $-80°C$ until analysis. An UPLC-single quadrupole-MS amino acid analysis system was combined with two separate UPLC-time-of-flight (TOF)-MS based platforms analyzing methanol serum extracts. 10 μL aliquots of the extracts prepared after methanol extract by adding 4 volumes of methanol were derivatized for amino acid analysison an Acquity-SQD system (Waters Corp., Manchester, UK). LCMS features (as defined by retention time, mass-to-charge ratio pairs, Rt-m/z), were associated with amino acids by comparison of their accurate mass spectra and chromatographic retention times in commercial serum metabolite extracts (Promocell inc., Germany) with those obtained using available reference standards. All data were processed using the TargetLynx application manager for MassLynx 4.1 (Waters Corp.) after intra- and inter-batch normalization, as previously described (Barr et al., 2012).

The immunohistochemical analysis of liver GLS1, GLS2 and glutamine synthetase expressions was assessed in a cohort of NASH patients and healthy controls recruited at the Department of Gastroenterology, Azienda Ospedaliero-Universitaria & University of Modena and Reggio Emilia, Modena, Italy. Patients show an average age of 42 ± 3 years and 38% of patients were female.

This study was approved by the Institutional Review Board of the Modena Province (n.2CEI-705; 08/04/2013) and was in accordance with the principles of the Declaration of Helsinki. Written informed consents were obtained from all participants, and characterized in Table S1. mRNA levels of *GLS1* were analyzed in liver biopsies of a cohort of patients with NASH and controls recruited at the Hospital Marqués de Valdecilla, Santander, Spain. Patients show an average age of 47 ± 3 years and 44% of patients were female. This study was approved by the Institutional Review Board of Cantabria (2012.095) and was in accordance with the principles of the Declaration of Helsinki. Written informed consents were obtained from all participants. Sample size estimation was made by using the "DSS Research sample size calculator." Even though both females and males were used an analysis of the influence was not performed as this significantly reduces sample size number.

Animal Maintenance
Male adult (three-month old) C57BL/6 mice were acquired from Charles River (St Germain sur l'Arbresle, France) and maintained and closely monitored at the AAALAC -accredited CIC bioGUNE animal facility on a 12/12 h light/dark cycle at 21 ± 1°C and humidity of 45 ± 10%. Eight-month male $Mat1a^{-/-}$ and their wild-type (WT) C57BL/6 littermates are bred at the animal facility of CIC bioGUNE. Animal procedures were approved by the CIC bioGUNE Institutional Animal Care and Use Committee and the Country Council of Bizkaia. Mice were maintained with *ad libitum* access to water and a diet devoid of choline with 0.1% methionine (0.1% MCDD) (A02082006i, Research Diets, Inc., New Jersey, USA) or a choline-deficient high-fat diet (CD-HFD) (D05010402, Research Diets Inc., New Jersey, USA). A control group was maintained on a regular diet with 1,030 mg/kg choline and 0.3% methionine (Teklad Global 14% Protein Rodent Maintenance diet; Envigo RMS Spain, Sant Feliu de Codines, Spain). In 0.1% MCDD and control diet, 17%–20% of calories are derived from protein, 10%–13% from fat and 63%–67% from carbohydrates while in the CD-HFD, 20% of calories are derived from protein, 45% from fat and 35% of carbohydrates.

Isolation and Culture of Primary Hepatocytes, Hepatic Stellate Cells (HSC) and Kupffer Cells (KC)
All animal experiments were performed according to the ARRIVE guidelines and carried out in accordance with the National Institutes of Health guide for the care and use of Laboratory animals (NIH Publications N0.8023, revised 1978) and the guidelines of European Research Council for animal care and use. Male mice were acquired from Charles River (St Germain sur l'Arbresle, France) and were maintained at the CIC bioGUNE Animal Facilities according to the criteria established by the European Union. In brief, mice were anesthetized with isoflurane (1.5% isoflurane in O$_2$), the abdomen was opened and a catheter was inserted into the vena cava. Liver was perfused with buffer A [1X PBS, 5 mM EGTA] (37°C, oxygenated) and portal vein was cut. Subsequently, liver was perfused with buffer B [1X PBS, 1mM CaCl$_2$, collagenase type I (Worthington)] (37°C, oxygenated). After the perfusion, liver was placed in a Petri dish containing buffer C [1X PBS, 2mM CaCl$_2$, 0.6% bovine serum albumin (BSA)] and disaggregated with forceps. Digested liver was filtered through sterile gauze. Then, mouse primary hepatocytes, KC and HSC were isolated either from healthy control or mice fed during 4 weeks a 0.1% MCDD as previously described (Zubiete-Franco et al., 2017). Briefly, perfused livers were centrifuged at 48g for 5 min. Supernatant was removed and hepatocytes present in pellet were resuspended in fresh 10%-fetal bovine serum (FBS; GIBCO) Minimun Essential Medium (MEM; GIBCO) containing penicillin (100 U/mL), streptomycin (100 U/mL), and glutamine (2 mM) (PSG; Invitrogen). Hepatocytes were plated on collagen-coated plates. Cell viability was validated by trypan blue exclusion test and more than 70% of viability was considered acceptable to proceed with the experiments. KC and HSC were further isolated from the supernatant by gradient centrifugation with Percoll Plus (GE Healthcare, Little Chalfont, United Kindgom) and selective adherence. Purity of primary hepatocytes, HSC and KC was determined by using a DNA agarose gel after PCR to identify albumin (Alb), α-smooth-muscle actin (αSMA) and F4/80, respectively.

THLE-2 Cell Line

The human liver epithelial cells acquired from ATCC® (isolated from adult from unknown sex) were cultured using BEGM from Lonza/ Clonetics Corporation, Walkersville, MD 21793 (BEGM Bullet Kit; CC3170), where we have discarded the gentamycin/ Amphotericin (GA) and Epinephrine and to which we add extra 5 ng/mL EGF, 70 ng/mL Phosphoethanolamine and 10% fetal bovine serum. Cells were grown at 37°C and 5%CO$_2$.

METHOD DETAILS

Treatments to Primary Mouse Hepatocytes and THLE-2 Cells

Upon attachment, isolated mouse primary hepatocytes were transfected by overnight incubation with 100 nM *Gls1* siRNA (QIAGEN, Madrid, Spain) using DharmaFECT 1 reagent (Dharmacon). Controls were transfected with an unrelated siRNA (QIAGEN, Madrid, Spain). Gene and protein knockdown were confirmed by RT-PCR and western blotting, respectively. Once attached, primary hepatocytes were maintained at 0% FBS MEM (GIBCO) overnight and were incubated during 24 or 48 h in Control media (MEM, GIBCO) or methionine and choline-deficient DMEM/F-12 media (custom-made MCD media, GIBCO). Isolated mouse hepatocytes were also treated with the GLS1 inhibitor Bis-2(5-phenylacetamido-1,3,4-thiadiazol-2-yl)ethyl sulfide (BPTES) (Sigma-Aldrich, St. QuentilFallavier, France). BPTES was dissolved in DMSO and used at a dose of 10μM. Lomitapide (N-(2,2,2-Trifluoroethyl)-9-[4-[4-[[[4′-(trifluoromethyl)[1,1′-biphenyl]2-yl]carbonyl]amino]-1 piperidinyl]butyl]9H-fluoren-9-carboxamde) (Sigma-Aldrich, St. QuentilFallavier, France), an inhibitor of VLDL export, that acts by inhibiting microsomal triglyceride transfer protein (MTP), was given to cells solubilized in DMSO at a concentration of 600 nM for a 24-h period. Oleic acid (Sigma-Aldrich, St. QuentilFallavier, France) conjugated to BSA at 400 μM was also given to hepatocytes during 6 h. Cells were grown at 37°C and 5%CO$_2$. Glutaminase inhibition after GLS1 pharmacological inhibitor treatment was confirmed by determining the amount of cellular glutamine and glutamate by UPLC-MS as explained below. Finally, cell viability after treatments was assessed using a caspase 3 activity assay as previously reported (Embade et al., 2012). Briefly, cells were lysed in caspase buffer and the protein content was determined by Bradford protein assay. 20 μL of 25x reaction buffer (PIPES pH 7.4 250 mM, EDTA 50 mM, 2.5% CHAPS, DTT 125 mM) were mixed with 2.5 μL of fluorogenic caspase-3 substrate (Enzo Life Sciences, USA) and with 10-50 μg of protein lysate in a total volume of 500 μl. The mixture was incubated at 37°C with gentle shaking for 5 h. Readings were taken at each h using a Spectramax M3 spectrophotometer (excitation wavelength 390 nm, emission wavelength 510 nm). Caspase 3 activity was determined by calculating the increase in fluorescence per h of incubation.

Treatments to Primary HSC and KC

HSC were cultured in 0% FBS RPMI-1640 Medium (GIBCO) and collected at different times after plating (0, 3, 5 and 7 days). KC were cultured in 0% FBS MEM (GIBCO) and stimulated with 200ng/mL lipopolyssacharide (LPS, Sigma) during 24 h. Cells were grown at 37°C and 5%CO$_2$.

Gls1 *Silencing* In Vivo *in 0.1% MCDD-Fed Rodents*

After two weeks of 0.1% MCDD, mice were randomly divided into two experimental groups: *in vivo* silencing of *Gls1* (si*Gls1*) or unrelated siRNA control (siCtrl), receiving 150 μL of 27 μM *Gls1*-specific siRNA (Custom Ambion® *In Vivo* siRNA) or control siRNA using Invivofectamine® 3.0 Reagent (Thermo Fisher Scientific) by tail vein injection. Tail vein injection was performed each three-four day interval until four weeks of dietary intervention. The mice were analyzed for transaminases and biochemistry in blood at 0, 2, and 4 weeks of exposure to the 0.1% MCDD. Serum samples were analyzed using a Selectra Junior Spinlab 100 analyzer (Vital Scientific, Dieren, Netherland) according to manufacturers' suggested protocol. At the day of sacrifice, four weeks after 0.1% MCDD, two different experiments were carried out.

Experiment 1. After overnight fast, animals were administered i.p. with (U-^{13}C)-glutamine 99% (Cambridge Isotope Laboratories, Inc., Andover, MA, USA) at 350 mg/kg, 20 min before sacrifice. Depending on the final purpose of the sample, livers were removed and either snap frozen in liquid nitrogen, optical coherence tomography cryocompound (OCT-)embedded, formalin fixed, or immediately analyzed as far as the experiment regarding the quantification of fatty acid β-oxidation (FAO) and Seahorse Analyzer experiments.

Experiment 2. In another group of animals, on the day of sacrifice mice were i.p. injected with poloxamer 407 (P-407) (Invitrogen, Carlsbad, CA, USA) in saline at 1 g/kg, as previously described (Millar et al., 2005). Blood was collected at baseline and six h after P-407 injection and triglycerides were quantified using a commercially available kit (A. Menarini Diagnostics, Italy). Six h after the P-407 injection, serum VLDL (d < 1.02 g/mL) were isolated by ultracentrifugation for 18-h at 35,000 rpm at 10°C in a Beckman Coulter Type 50.4 Ti Rotor. Lipids content on VLDL were extracted as described previously (Folch et al., 1957) and separated by thin layer chromatography (Ruiz and Ochoa, 1997). From the total volume of extracted VLDL, 60% was used for lipid extraction. For lipid extraction, the correspondent volume of VLDL and up to 1.5 mL of dH$_2$O were mixed with 8 mL of chloroform:methanol:HCl (2:1:0.0075, v/v) solution (Scharlau Chemicals, Spain). Tubes were vigorously shaken with a vortex for 2 min. Then, they were centrifuged at 1,000 xg for 15 min at 4°C to separate the aqueous phase from the organic phase. The organic phase was transferred to another extraction tube using a glass pasteur pipette. Lipids from the upper phase were reextracted. For reextraction, 4 mL of chloroform:methanol:HCl (2:1:0.0075, v/v) were added and the tubes were vigorously shaken for 2 min and centrifuged at 1,000 xg for 10 min at 4°C. The organic phase was mixed with the previously obtained one. For the removal of aqueous contaminant, the chloroform extract was washed with the third part of the total volume of KCl 0.88% solution. Each tube was shaken for 1 min and

centrifuged for 10 min at 1,000 xg and the lower phase was transferred to another extraction tube. Finally, the chloroform was evaporated in a concentrator- evaporator. Lipids were dissolved in 200 μL of toluene and kept at -20°C in N_2 atmosphere until processing. The lipid separation was performed by thin layer chromatography (TLC), performing a six chromatographic developments. First, the silica-gel plates of 20 $\times$ 20 cm ("Pre-coated TLC-plates SIL-G25," Macherey-Nagel) were pre-treated with 1 $^{mM\ EDTA-Na}_2$. Silica-gel plates were left drying overnight and washed with chroloform:methanol:dH2O (60:40:10, v/v/v) overnight. The following day, the plates were activated at 100°C for 30 min. Then, 3 μL of pure lipid mixtures (Avanti Polar Lipids, USA and Sigma-Aldrich) of known lipid concentrations and 1 or 3 μL of the lipid extracts from the samples were applied at 1.5 cm from the lower edge of the plate. Lipid quantities (nmol) for calibration were as next described: Cholesteryl ester (CE) (0.09-1.45), triglycerides (TG) (0.27-17), diglycerides (DG) (0.15-3), free cholesterol (FC) (0.36-3.6), phosphatidylethanolamine (PE) (0.33-3.91), phosphatidylinositol (PI) (0.1-1.72), phosphatidylserine (PS) (0.13-2.22) and phosphatidylcholine (PC) (0.63-7.63). Six chromatographic developments were carried out in solutions of decreasing polarity as presented in the Table S4. After each chromatographic development, the plates were dried using hot air. When the chromatographic separations were performed, the plate was stained immersing in a CuSO4 solution at 10% (p/v) in H3PO4 at 8% (v/v) for 10 s. After, plates were dried with hot air and plates were developed for 3 min at 200°C. The image of the TLC plate was digitalized using the densitometer GS-800 and quantification was performed with Quantity One software. The integrated optic density (IOD) of each lipid, was interpolated in the IOD values of the calibration curves. For the analysis of the VLDL apoB, 0.3% of the secreted VLDL was used for western blotting. Since there are no proteins to use as loading control in the VLDL population, ponceau red staining was performed as a loading control.

Gls1 *Silencing* In Vivo *in CD-HFD-Fed Rodents*

After three weeks of CD-HFD, mice were randomly divided into two experimental groups, si*Gls1* and siCtrl. Tail vein injection was performed each three-four day interval until six weeks of dietary intervention. For analysis of triglycerides content in circulating VLDL particles, serum VLDLs (d < 1.02 g/mL) were isolated from the cava vein after 2 h fasting. VLDL isolation was performed as described above. Quantification of TG content in VLDL was assessed using a commercially available kit (A. Menarini Diagnostics, Italy).

RNA Isolation and Quantitative Real-Time Polymerase Chain Reaction

Total RNA was isolated with Trizol (Invitrogen). One to two μg of total RNA was treated with DNase (Invitrogen) and reverse transcribed into cDNA using M-MLV Reverse Transcriptase (Invitrogen). Quantitative real-time PCR (RT-PCR) was performed using SYBR® Select Master Mix (Applied Biosystems) and the Viia 7 Real-Time PCR System (Applied Biosystems). The Ct values were extrapolated to a standard curve, and data was then normalized to the housekeeping expression (*Arp*). Primers sequences are described in Table S5.

Immunohistochemistry

Paraffin embedded liver samples were sectioned, dewaxed and hydrated. All procedures were performed according to standard protocols using the EnVision+ System HRP (Dako, Denmark). Samples were incubated with Vector Vip substrate (Vectorlabs, Burlingame, USA) for color development. Five to ten random images per sample were taken blinded using an AXIO Imager A1 microscope (Carl Zeiss AG, Jena, Germany). Stained area percentage of each sample was calculated using FIJI (ImageJ). Stainings was performed according to Table S5.

Immunofluorescence

Paraffin-embedded liver samples were rehydrated, unmasked with the conditions described in Table S6, followed by the incubation with 2.5% goat serum for 30 min. The primary antibody and the corresponding secondary antibody were then incubated according to Table S5. Nuclei were counterstained with Fluoromount-G with DAPI (Southern Biotech). The slides were mounted with Fluoromount-G (Southern Biotech) containing DAPI and representative images were taken using an Upright fluorescent microscope (Axioimager D1).

H&E and Sirius Red staining

We have stained for hematoxylin and eosin (H&E) and Sirius Red staining for collagen in paraffin-embedded sections of formalin-fixed liver samples. Samples were initially deparaffinised in Histo-Clear (Electron Microscopy Sciences, Hatfield. PA, USA) and rehydrated through graded alcohol solutions. After the deparaffinization and rehydration process, sections were subjected to conventional hematoxylin and eosin or Sirius red stainings. For H&E staining, sections were stained with Harris Hematoxylin (Bio-Optica, Milano, Italy) for 15 min followed by eosin staining (Sigma Aldrich) for 15 min. Washed in running tap water for 5 min and differentiated in 0.5% HCl for 1 s. Samples are then dehydrated in graded alcohol solutions until 100% and mounted in DPX mounting medium (Sigma Aldrich). For Sirius Red staining, rehydrated sections were then stained with Sirius red solution 1 (0.01% Fast Green FCF in picric acid, Sigma Aldrich) for 20 min and then with Sirius red solution 2 (0.04% Fast Green FCF/0.1% Sirius red in picric acid, Sigma Aldrich) for another 15 min. After the respective staining, sections were then dehydrated directly in 100% alcohol and mounted in DPX mounting medium (Sigma Aldrich). F4/80, a membrane macrophage marker, immunohistochemical staining was used. For α-SMA, a marker of activated HSC, immunofluorescence was used.

Liver Sudan Red Staining

For the histological quantification of hepatic lipids we have used Sudan Red staining. Briefly, cut liver cryostat section of 8 microms were incubated with freshly-prepared Sudan III stain (Sigma-Aldrich) and contrasted with Mayers hematoxylin. Hepatic ammonia

content was quantified by using a methodology recently described by our group (Gutiérrez-de-Juan et al., 2017). Five to ten random images per sample were taken blinded using an AXIO Imager A1 microscope (Carl Zeiss AG, Jena, Germany). Stained area percentage of each sample were calculated using FIJI (ImageJ).

Protein Isolation and Western Blotting

Total protein extracts from primary hepatocytes and hepatic tissue were resolved in sodium dodecyl sulfate-polyacrylamide gels and transferred to nitrocellulose membranes. As secondary antibodies, we used anti-rabbit-IgG-HRP-linked (Cell Signaling) and anti-mouse IgG-HRP-linked (Cell Signaling). The antibodies and conditions used for Western Blotting are described in Table S6.

BODIPY Staining in Isolated Mouse Hepatocytes

Hepatocytes in culture were collected in covers and incubated with boron-dipyromethene (BODIPY 493/503) (Molecular Probes, Thermo Fisher Scientific) at a concentration of 10μg/mL during 45 min after fixation in 4% paraformaldehyde for 10 min. Quantification of lipid bodies was performed using FIJI (ImageJ).

Quantification of Hepatic Lipids

Liver triglycerides were quantified after extraction using a published method (Pitman et al., 2011). Briefly, pieces of mouse liver were weighed, then homogenized in 10X of PBS 1X. The homogenates were then extracted with a 2:1 (v:v) mixture of chloroform-methanol by vortexing thoroughly. Samples were then centrifuged at 4,200 g at $4°C$ for 10 min. The organic (lower) phase was air-dried in a fresh tube then resuspended in 100 μL of 1% Triton X-100 in ethanol. This was then air-dried and resuspended in 500 μL 1 × PBS, for the final lipid extract. After extraction, aliquots of this extract were used to measure triglycerides using an automatized Selectra Junior Spinlab 100 analyzer (Vital Scientific, Dieren, Netherland. For the quantification of fatty acids, liver tissues (30 mg) were homogenized with 10 volumes of ice-cold phosphate buffered saline (1XPBS) in a Potter homogenizer (20 strokes). Fatty acids were measured in homogenates using a kit from Wako Chemicals (Richmond, VA). Hepatic total phospholipids were quantified by using a commercially available kit from Sigma-Aldrich (St. QuentilFallavier, France). Families of phospolipids were extracted from 1.5 mg of protein from homogenates (Folch et al., 1957) and were quantified as described previously (Ruiz and Ochoa, 1997). Lipid extraction from liver homogenates was performed as explained above but here from 1.5 mg of protein from the homogenate. 3 or 8 μL from the lipid extracts were separated by TLC as explained above.

Quantification of Lipids in Primary Hepatocytes

Triglycerides in primary hepatocytes were measured after extraction by following a modification of an already existing protocol (García-Ruiz I et al., 2014). Briefly, samples were washed in cold PBS and resuspended in 500 μL of 5% NP-40/ddH2O solution to be heated at $95°C$ during 5 min. The samples were analyzed using a Selectra Junior Spinlab 100 analyzer (Vital Scientific) according to manufacturers' suggested protocol.

Determination of Cellular Reactive Oxygen Species (ROS)

Cellular ROS production in mouse primary hepatocytes was assessed using CellROX Deep Green Reagent (Thermo Fisher Scientific). Briefly, hepatocytes were loaded with 1.5 μM CellROX in 10% FBS MEM for 30 min at $37°C$ in a CO_2 incubator. The hepatocytes were then carefully washed three times with 1XPBS, collected and analyzed by flow cytometry FACS Canto II (BD Biosciences).

Determination of Mitochondrial Reactive Oxygen Species (ROS)

Mitochondrial ROS production in primary hepatocytes was assessed using MitoSOX Red mitochondrial superoxide indicator (Invitrogen, USA). The cells were loaded with 2 μM MitoSOX Red for 10 min at $37°C$ in a CO_2 incubator. The cells were then washed three times with PBS. Fluorescence was read at 510 nm (excitation) and 595 (emission) using a plate reader SpectraMax M2 (bioNova).

Lipid Peroxidation Assay Kit

Malondialdehyde (MDA), together with 4-hydroxynonenal (4-HNE), is a natural bi-product of lipid peroxidation and its quantification is generally used as marker for lipid peroxidation. The MDA in the sample reacts with thiobarbituric acid (TBA) to generate a MDA-TBA adduct. The MDA-TBA adduct can be easily quantified colorimetrically (OD = 532 nm) MDA content in liver samples was quantified by using a commercially available kit from Sigma-Aldrich (St. QuentilFallavier, France).

Hepatic Fatty Acid Oxidation (FAO)

Fatty acid β-oxidation was assessed as described before (Gao et al., 2015; Hirschey et al., 2010; Porteiro et al., 2017). Fresh liver pieces were homogenized in a Potter homogenizer (5 strokes) in cold buffer (25 mM Tris-HCl, 500 nM sucrose, 1 mM EDTA-Na$_2$ pH 7,4) and sonicated for 10 s. Then, the homogenates were centrifuged at 500 xg for 10 min at $4°C$. Approximately 500 μg of protein from the homogenates supernatant was used for the assay in a volume of 200 μl. The reaction started by adding 400 μl of assay mixture containing 0.5 μCi/mL [1-^{14}C] palmitic acid to the samples and was incubated for 1 h at $37°C$ in eppendorf tubes with a Whatman paper circle in the cap. The reaction was stopped by adding 300 μl of 3 M perchloric acid and 1 M NaOH was added to impregnate the whatman cap. After 2 h the Whatman caps were retired and the radioactivity associated was measured in a scintillation

counter. The eppendorf tubes were centrifuged at 21,000 xg 10 min at 4°C. 400 μl from the supernatant were collected and the radio-activity was counted in a scintillation counter. The supernatant contained the acid soluble metabolites (ASM) and the Whatman caps captured the released CO_2.

Respiration Studies in Liver Mitochondria

The respiration of liver mitochondria was measured at 37°C by high-resolution respirometry with the Seahorse Bioscience XF24-3 Extracellular Flux Analyzer. Liver mitochondria were isolated as recommended by Agilent Seahorse Application note. Succinate (10 mM) and rotenone (2 μM) were used as substrates to quantify State 2. State 3 was initiated with ADP, State 4 induced with the addition of oligomycin (State 4o), and FCCP-induced maximal uncoupler-stimulated respiration (State 3u) were sequentially measured. The normalized data were expressed as pmol of O_2 per minute or milli-pH units (mpH) per minute, per μg mitochondrial protein.

Glutaminase Activity

Glutaminase activity was determined *in vivo* from mouse liver tissue as well as *in vitro* in primary cultured hepatocytes. To assess glutaminase activity in mouse liver, we have calculated the ratio between $^{13}C_5$-glutamate and $^{13}C_5$-glutamine after i.p. injection of $^{13}C_5$-glutamine (20 min before sacrifice. Semi-quantification of the labeled metabolites was performed by UPLC-MS. Glutaminase activity in hepatocytes was measured after 48 h incubation with methionine/choline deficient media (MCD) and treatment with siRNA against GLS1 (si*Gls1*) or unrelated control (siCtrl) overnight. The concentration of glutamate and glutamine per μg protein was determined by LCMS and the ratio between the concentrations was taken as a measure for glutaminase activity. LCMS and extraction procedures are described below.

Tricarboxylic Acid (TCA) Cycle Activity

An i.p. injection of $^{13}C_5$-glutamine was given to animals fed a 0.1% MCDD 20 min before sacrifice. Upon these conditions, accumulation of the citrate metabolite and more importantly the ratio between $^{13}C_1$-citrate and $^{13}C_5$-glutamine were measured by LCMS after extraction.

Incorporation of $^{13}C_6$-glucose in Ptd-Cho in Isolated Mouse Hepatocytes

Isolated mouse hepatocytes (5x10^5 cells) were incubated with MCD medium, MCD medium combined with siRNA against *Gls1* or normal medium for 24 h. To each treatment either labeled $^{13}C_6$-glucose or non-labeled glucose was added in a concentration of 10 mM.

LCMS Sample Preparation

Two types of biological material were analyzed with LCMS, namely liver tissue and primary cultured hepatocytes. All liver extractions were carried out in the same manner with a method that was optimized for polar metabolites. On the other hand, hepatocyte extraction methods depended on the metabolite type of interest i.e., being polar or apolar metabolites. The polar metabolite set consisted of GSH, GSSG, glutamine, glutamate and citrate. The apolar set consisted of the following panel of phosphatidylcholines: PC(32:0), PC(32:1), PC(34:1), PC(34:2) and PC(36:2). In short, liver tissues for the determination of glutaminase and TCA cycle activity and levels of GSSG and GSH (polar metabolite set) were homogenized in 500 μL of ice-cold extraction liquid (EL) with a tissue homogenizer (FastPrep) in a 40 s cycle at 6000 rpm. The EL consisted of a mixture of methanol/water (50/50%v/v) with 10 mM acetic acid. Next 400 μL of homogenate was transferred into a new aliquot and shaken for 30 min at 1400 rpm and centrifuged for 30 min at 14000 rpm at 4°C. Next, 75 μL of the supernatant was transferred to a fresh aliquot and stored at −80°C for 30 min. The chilled supernatants were evaporated with a speedvac in approximately 2 h. The resulting pellets were resuspended in 250 μL water/acetonitrile(MeCN)/formic acid (FA) (39.9/60/0.1%v/v/v, resuspension liquid RL). These resuspensions were transferred to glass vails for LCMS analysis.

Hepatocytes were extracted as follows. Cell pellets were collected and lysed in 500 μL EL. Homogenization was performed with a tissue homogenizer (Precellys) in two 30 s cycles at 6000 rpm. Subsequently 400 μL of the homogenate was transferred to a new aliquot and shaken at 1400 rpm for 30 min at 4°C. Next the aliquots were centrifuged for 15' at 14000 rpm at 4°C. Three aliquots of 75 μL per sample (225 μL) of the supernatant were transferred to fresh aliquots and placed at −80°C for 20'. The chilled supernatants were evaporated with a speedvac in approximately 2 h. The resulting pellets (3 per sample) were serially resuspended in 150 μL RL.

To extract Ptd-Cho from hepatocytes to 400 μL of homogenate, obtained as described above, another 400 μL of chloroform was added. The resulting solution was shaken at 1400 rpm for 1 h at 4°C. Next, the aliquots were centrifuged for 30 min at 14000 rpm at 4°C in order to separate the phases. From the organic phase (chloroform) 200 μL per sample was transferred to fresh aliquots and placed at −80°C for 20 min and evaporated with a speedvac. The resulting pellets were resuspended in 150 μL pure methanol.

Liquid Chromatography and Mass Spectrometry Methods

Liquid chromatography-coupled mass spectrometry (LCMS) was used to determine activity of the tricarboxylic acid (TCA) cycle in liver, relative levels of reduced or oxidized glutathione (GSH and GSSG respectively) in liver, glutaminase activity in liver and hepatocytes and incorporation of $^{13}C_6$-glucose in Ptd-Cho hepatocytes.

The LCMS instrumentation consisted of an Acquity-SQD UPLC system (Waters Corp., Manchester) coupled to a SYNAPT G2 HDMS Time of Flight mass spectrometer (Waters Corp.). For all performed assays the following MS settings were kept constant. The ion source temperature was 120°C and capillary temperature 450°C. The flow of the cone and desolvation gas (both nitrogen) were set to 5 L/h and 600 L/h, respectively. A 2 ng/mL leucine-enkephalin solution in RL was infused at 10 μL/min and used for a lock mass to automatically correct deviations in mass accuracy. This signal was measured approximately each 30 s for 0.5 s.

Two different LCMS methods were used to measure either polar or apolar metabolites. Metabolites from the polar set were separated prior to MS analysis under the following conditions. Chromatography was performed on a 2.1 × 100 mm, 1.7 μm BEH amide column (Waters Corp.), thermostated at 40°C. Mobile phase solvent A (aqueous phase) containedf 99.5% water, 0.5% FA and 20 mM ammonium formate while solvent B (organic phase) contained 29.5% water, 70% MeCN, 0.5% FA and 1 mM ammonium formate. In order to obtain a good separation of the analytes, the following gradient was used: from 5% A to 50% A in 2.4 min in curved gradient (#8, as defined by Waters), from 50% A to 99.9% A in 0.2 min constant at 99.9% A for 1.2 min, back to 5% A in 0.2 min. The flow rate was 0.250 mL/min and the injection volume was 2 μL. All samples were injected randomly. After every 8 injections a QC low and QC high were injected. All samples were injected in duplicate. The MS was operated in positive and negative electrospray ionization (+ESI, -ESI) in full scan mode depending on the analyte. Citrate, glutamate and glutamine were measured in ESI- and glutathione in ESI+. The cone voltage was 25 V and capillary voltage was 250 V in +ESI and 500 V in -ESI.

As for the apolar set a 1 × 100 mm, 1.7 μm BEH C18 column (Waters Corp.), thermostated at 60°C, was used to separate the analytes before entering the MS. Solvent A (aqueous phase) consisted of 40% water, 60% MeCN 10 mM ammonium formate while solvent B (organic phase) consisted of 10% MeCN, 90% isopropanol and 10 mM ammonium formate. The following gradient was used: from 50%A to 1%A in 4 min in a curved gradient (#8, as defined by Waters), constant at 1%A for 0.8 min, back to 50%A in 0.2 min. The flow rate was 0.120 mL/min and the injection volume was 2 μL. All samples were injected randomly. After every 8 injections a QC sample (pooled samples) was injected. The mass spectrometer was operated ESI+ with a capillary voltage of 250 V.

LCMS Data Analysis

Extracted ion traces (XICs) were obtained and integrated for specific analytes in a 20 mDa integration window and subsequently smoothed and integrated with QuanLynx software (Waters Corp.). For GSH the XIC was determined at an m/z = 308.0916, for GSSG at m/z = 613.1598, for citric acid at m/z 191.0192, for $^{13}C_1$-citric acid at m/z 192.0225, for glutamine at m/z 145.0613, for $^{13}C_5$-glutamine at m/z 150.0781, for glutamate at m/z 146.0453, for $^{13}C_5$-glutamate at m/z 151.0621.

As for the Ptd-Cho species it was found that labeling via $^{13}C_6$-glucose introduced three ^{13}C atoms in these phospholipids. Therefore the following XICs were extracted: PC(32:0) at m/z 734.57 and 737.58005, PC(32:1) at m/z 732.5543 and 735.56435, PC(34:1) at m/z 760.5864 and 763.59645, PC(34:2) at m/z 758.57 and 761.58005, PC(36:2) at m/z 786.6013 and 789.61135.

As for labeling experiments, since the m/z values of ^{13}C-labeled species can overlap with the natural occurring isotopes in a 20 mDa window, the signals of the ^{13}C-labeled species needed to be corrected. Therefore, an isotope model of the endogenous metabolite was made with the Isotope Model tool in MassLynx software (Waters Corp.). Next, the absolute abundances of naturally occurring isotopes were estimated by taking the chromatographic peak intensities of the most abundant spectral peak representing the endogenous species and multiplying that by the relative abundances of the natural isotopes. These numbers were than subtracted from the integrated signal of the ^{13}C-isotopes with the same mass as the naturally occurring ones. The following equation describes these calculations:

$$S_{m,isotope} = S_{m,total} - d_{m,natural}S_0$$

where $S_{m,isotope}$ is the signal (area or height) of the ^{13}C-isotope with mass m ± 20 mDa (integration window) of a specific analyte, $S_{m,total}$ is the measured signal at mass m ± 20 mDa, $d_{m,natural}$ is the relative abundance of the natural occurring isotope with mass m (the abundance of the most abundant signal representing the analyte is set to 1) and S_0 is the signal of the natural occurring metabolite with the highest spectral peak. Finally, the corrected signals were normalized on tissue weight or μg protein.

QUANTIFICATION AND STATISTICAL ANALYSIS

Statistical significance was determined by using Prism 5 (GraphPad Software). The Grubb's outlier test was performed by using the GraphPad, Prism8 software, and no value was excluded. One-way analysis of variance (ANOVA) followed by post hoc Bonferroni test was used in case 3 groups were compared or using the Student's t test in case 2 groups were compared. A $p < 0.05$ was considered statistical different. Statistic parameters are reported in figure legends.

DATA AND CODE AVAILABILITY

This study did not generate any unique datasets or code.